J|A|C|S
ARTICLES
Published on Web 10/16/2002

The Nature of Solid-State N−H···O/O−H···N Tautomeric Competition in Resonant Systems. Intramolecular Proton Transfer in Low-Barrier Hydrogen Bonds Formed by the ···O=C−C=N−NH··· ⇄ ···HO−C=C−N=N··· Ketohydrazone−Azoenol System. A Variable-Temperature X-ray Crystallographic and DFT Computational Study

Paola Gilli,[†] Valerio Bertolasi,[†] Loretta Pretto,[†] Antonín Lyčka,[‡] and Gastone Gilli*,[†]

Contribution from the Centro di Strutturistica Diffrattometrica and Dipartimento di Chimica, Università di Ferrara, I-44100 Ferrara, Italy and Research Institute for Organic Syntheses, CZ-53218 Pardubice-Rybitvi, Czech Republic

Received April 24, 2002

Abstract: The tautomeric ···O=C−C=N−NH··· ⇄ ···HO−C=C−N=N··· ketohydrazone−azoenol system may form strong N−H···O/O−H···N intramolecular resonance-assisted H-bonds (RAHBs) which are sometimes of the low-barrier H-bond type (LBHB) with dynamic exchange of the proton in the solid state. The problem of the N−H···O/O−H···N competition in these compounds is studied here through variable-temperature (100, 150, 200, and 295 K) crystal-structure determination of ***pF*** = 1-(4-F-phenylazo)2-naphthol and ***oF*** = 1-(2-F-phenylazo)2-naphthol, two molecules that, on the ground of previous studies (Gilli, P; Bertolasi, V.; Ferretti, V.; Gilli, G. *J. Am. Chem. Soc.* **2000**, *122*, 10405), were expected to represent an almost perfect balance of the two tautomers. According to predictions, the two molecules form remarkably strong bonds (d(N···O) = 2.53−2.55 Å) of double-minimum or LBHB type with dynamic N−H···O/O−H···N exchange in the solid state. The enthalpy differences between the two minima, as measured by van't Hoff methods from the X-ray-determined proton populations, are very small and amount to $\Delta H° = -0.120$ and $\Delta H° = -0.156$ kcal mol^{-1} in favor of the N−H···O form for ***pF*** and ***oF***, respectively. Successive emulation of ***pF*** by DFT methods at the B3LYP/6-31+G(d,p)//B3LYP/6-31+G(d,p) level has shown that both energetic and geometric experimental aspects can be almost perfectly reproduced. Generalization of these results was sought by performing DFT calculations at the same level of theory along the complete proton-transfer (PT) pathway for five test molecules designed in such a way that the RAHB formed changes smoothly from weak N−H···O to strong O−H···N through very strong N−H···O/O−H···N bond of LBHB type. A systematic correlation analysis of H-bond energies, H-bond and π-conjugated fragment geometries, and H-bond Bader's AIM topological properties performed along the PT-pathways leads to the following conclusions: (a) any X−H···Y H-bonded system is fully characterized by its intrinsic PT-barrier, that is, the symmetric barrier occurring when the proton affinities of X and Y are identical; (b) the intrinsic X−H···Y bond associated with the symmetric barrier is the strongest possible bond in that system and will be single-minimum (single-well, no-barrier) or double-minimum (double-well, low-barrier) according to whether the intrinsic PT-barrier is lower or slightly higher than the zero-point vibrational level of the proton; (c) with reference to the intrinsic H-bond, the effect of chemical substitution can only be that of making more and more dissymmetric the PT-barrier, while the two H-bonds split in a higher-energy bond which is stronger because closer to the transition-state structure and in a lower-energy one (the stable form) which is weaker because farther from it; (d) complete dissymmetrization of the PT-barrier will increasingly weaken the more stable H-bond until the formation of an extreme dissymmetric single-minimum or dissymmetric single-well H-bond.

Introduction

N−H···O/O−H···N competition is characteristic of two well-distinguished H-bonded chemical systems:

(i) Positive/negative charge-assisted H-bonds [(±)CAHB][1] related to the AcO−H···N≡ ⇄ AcO$^-$···H−N$^+$≡ acid−base equilibrium where the proton is shifted on the O or N side according to the relative pK_a values of the AcOH organic or inorganic acid and of the ≡N−H$^+$ conjugated acid of an organic nitrogen base.[1a,2] Very strong H-bonds of this type are charac-

* Address correspondence to this author. Address: Dipartimento di Chimica, Università di Ferrara, Via L. Borsari, 46, 44100 Ferrara (Italy). E-mail: ggilli.chim@unife.it. Tel.: +39-0532 291141. Fax: +39-0532 240709.
[†] Università di Ferrara.
[‡] Research Institute for Organic Syntheses.

(1) (a) Gilli, G.; Gilli, P. *J. Mol. Struct.* **2000**, *552*, 1. (b) Gilli, P.; Bertolasi, V.; Ferretti, V.; Gilli, G. *J. Am. Chem. Soc.* **2000**, *122*, 10405.

10.1021/ja020589x CCC: $22.00

terized by a close matching of the acid and base pK_a (or correlated proton affinity, PA) values and have been indicated as low-barrier H-bonds (LBHB).[3]

(ii) Resonance-assisted H-bonds (RAHB)[4] related to the $\cdots O = R_n - NH \cdots \rightleftarrows \cdots HO - R_n = N \cdots$ equilibrium, where R_n (n odd) is a resonant spacer[5] of n atoms forming a chain of alternating single and double bonds. The most studied are the intramolecular R_3–RAHBs formed by the enaminone−iminoenol (**I**), ketohydrazone−azoenol (**II**), and nitrosoenamine−iminooxime (**III**) resonant fragments.[1b,6a−c] Data so far collected show that the H-bonds in **I**−**III** share two interesting features. First, the intramolecular H-bond is almost inevitably of the N−H···O type. Second, the bond formed displays N···O distances (e.g., $2.60 \leq d(N \cdots O) \leq 2.70$ Å in simple enaminones **I**)[1b] which, though shorter than in the nonresonant case ($d(N \cdots O) > 2.70$ Å), are significantly longer than the corresponding O···O distances found in β-diketone enols forming an equivalent intramolecular O−H···O bond of resonant type ($2.37 \leq d(O \cdots O) \leq 2.59$ Å for the intramolecular case).[5b,c]

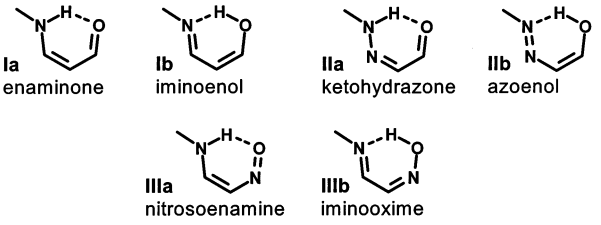

The present paper is specifically devoted to the study of molecules forming these intramolecular N−H···O bonds of the R_3–RAHB class, and it is aimed at determining the factors affecting their strength, the single-minimum or double-minimum shape of the potential experienced by the H-bonded proton, and finally the factors that may switch the system from its N−H···O to O−H···N form. Previous work on this system has shown that the H-bonds formed can be interpreted in terms of the so-called electrostatic-covalent H-bond model[1,4c] according to which the N−H···O bond is not simply an electrostatic interaction but contains a part of covalency in view of the mixing of the two VB resonance forms **IVa** ↔ **IVb**, which is the more efficient the more alike the PA (or related pK_a) values of the H-bond donor and acceptor groups, or alternatively the energies of the two VB wave functions Ψ(**IVa**) and Ψ(**IVb**)[1a], are. On these grounds, it is easy to predict[1] that (i) the intrinsic weakness of the heteronuclear N−H···O bond in respect to the O−H···O homonuclear one is to be imputed to the inefficient mixing of the N−H···O (**IVa**) and O−H···N (**IVb**) VB resonance forms because of the greater PA of nitrogen with respect to oxygen or because of the greater stability of Ψ(**IVa**) with respect to Ψ(**IVb**); (ii) any resonant N−H···O bond can be strengthened by chemical substituents able to lower PA(N) by electron attraction or to rise PA(O) by electron donation or, alternatively, to destabilize Ψ(**IVa**) or stabilize Ψ(**IVb**).

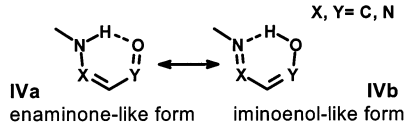

Applicability of rule ii has been extensively investigated for both intramolecular[1] and intermolecular[6d] N−H···O R_3−RAHBs, for which several strengthening (or weakening) substituents were indicated. The most efficient way for strengthening the N−H···O RAHB and, eventually, switching it to the O−H···N form turned out to be that of taking advantage of the resonance energy of aromatic rings fused with the R_3–RAHB fragment as indicated, for the ketohydrazone series, in schemes **V**−**VII**. For this series, the rather weak N−H···O bond in **V** can be switched to a stronger O−H···N one in **VI** by condensation with a phenyl ring, which greatly stabilizes form **b** because the phenyl resonance energy would be lost in form **a**. Condensation with a naphthalene ring (**VII**) is expected to produce a situation intermediate between **V** and **VI** because of the smaller resonance energy associated with a single naphthalene aromatic ring, and in fact, the two tautomers **VIIa** and **VIIb** are nearly isoenergetic and liable to form much stronger N−H···O bonds most probably of the LBHB type.

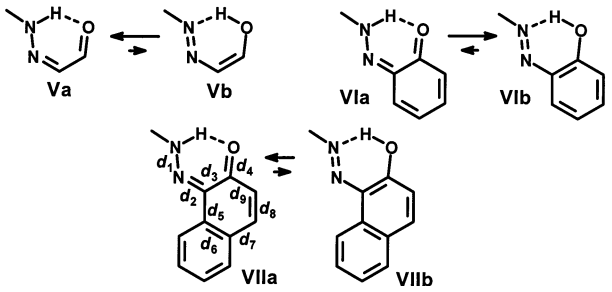

Experimental data so far collected[1,6,7] widely support these considerations: N···O distances are systematically shorter in **VI** and **VII** than in **V**, while **V** and **VI** are normally found to prefer N−H···O and O−H···N forms, respectively. Less clear is where the proton is located in **VII**. X-ray crystal data indicate a large prevalence of N−H···O bonds, though a few cases of

(2) (a) Meot-Ner (Mautner), M. *J. Am. Chem. Soc*. **1984**, *106*, 1257. (b) Meot-Ner (Mautner), M. In *Molecular Structure and Energetics*; Liebman, J. F., Greenberg, A., Eds.; VCH: Weinheim, 1987; Vol. IV, Chapter 3. (c) Zeegers-Huyskens, T. *J. Mol. Struct.* **1986**, *135*, 93. (d) Zeegers-Huyskens, T.; Huyskens, P. L. In *Intermolecular Forces*; Huyskens, P. L., Luck, W. A., Zeegers-Huyskens, T., Eds.; Springer-Verlag: Berlin, 1991; Chapter 1. (e) Zeegers-Huyskens, T. In *Intermolecular Forces*; Huyskens, P. L., Luck, W. A., Zeegers-Huyskens, T., Eds.; Springer-Verlag: Berlin, 1991; Chapter 6. (f) Malarski, Z.; Rospenk, M.; Sobczyk, L.; Grech, E. *J. Phys. Chem*. **1982**, *86*, 401. (g) Sobczyk, L. *Ber. Bunsen-Ges. Phys. Chem.* **1998**, *102*, 377. (*h*) Pan, Y.; McAllister, M. A. *J. Org. Chem.* **1997**, *62*, 8171.

(3) (a) Cleland, W. W. *Biochemistry* **1992**, *31*, 317. (b) Cleland, W. W.; Kreevoy, M. M. *Science* **1994**, *264*, 1887. (c) Frey, P. A.; Whitt, S. A.; Tobin, J. B. *Science* **1994**, *264*, 1927. (d) Cleland, W. W.; Frey, P. A.; Gerlt, J. A. *J. Biol. Chem*. **1998**, *273*, 25529. (e) Harris, T. K.; Mildvan, A. S. *Proteins* **1999**, *35*, 275. (f) Frey, P. A. *Magn. Reson. Chem.* **2001**, *39*, S190. (g) Perrin, C. L.; Ohta, B. K. *J. Am. Chem. Soc.* **2001**, *123*, 6520.

(4) (a) Gilli, G.; Bellucci, F.; Ferretti, V.; Bertolasi, V. *J. Am. Chem. Soc.* **1989**, *111*, 1023. (b) Bertolasi, V.; Gilli, P.; Ferretti, V.; Gilli, G. *J. Am. Chem. Soc*. **1991**, *113*, 4917. (c) Gilli, P.; Bertolasi, V.; Ferretti, V.; Gilli, G. *J. Am. Chem. Soc*. **1994**, *116*, 909. (d) Bertolasi, V.; Gilli, P.; Ferretti, V.; Gilli, G. *Chem. Eur. J.* **1996**, *2*, 925.

(5) (a) Gilli, G.; Bertolasi, V.; Ferretti, V.; Gilli, P. *Acta Crystallogr*. **1993**, *B49*, 564. (b) Gilli, P.; Ferretti, V.; Bertolasi, V.; Gilli, G. In *Advances in Molecular Structure Research*; Hargittai, I., Hargittai, M., Eds.; JAI Press Inc.: Greenwich, CT, 1996; Vol. 2, p 67. (c) Gilli, P.; Ferretti, V.; Gilli, G. In *Fundamental Principles of Molecular Modeling*; Gans, W., Amann, A., Boeyens, J. C. A., Eds.; Plenum Press: New York, 1996.

(6) (a) Bertolasi, V.; Ferretti, V.; Gilli, P.; Gilli, G.; Issa, Y. M.; Sherif, O. E. *J. Chem. Soc., Perkin Trans. 2* **1993**, 2223. (b) Bertolasi, V.; Nanni, L.; Gilli, G.; Ferretti, V.; Gilli, P.; Issa, Y. M.; Sherif, O. E. *New. J. Chem.* **1994**, *18*, 251. (c) Bertolasi, V.; Gilli, P.; Ferretti, V.; Gilli, G.; Vaughan, K. *New J. Chem.* **1999**, *23*, 1261. (d) Bertolasi, V.; Gilli, P.; Ferretti, V.; Gilli, G. *Acta Crystallogr*. **1998**, *B54*, 50.

(7) (a) Krygowski, T. M.; Wozniak, K.; Anulewicz, R.; Pawlak, D.; Kolodziejski, W.; Grech, E.; Szady, A. *J. Phys. Chem. A* **1997**, *101*, 9399. (b) Filarowski, A.; Koll, A.; Glowiak, T.; Majewski, E.; Dziembowska, T. *Ber. Bunsen-Ges. Phys. Chem.* **1998**, *102*, 393. (c) Filarowski, A.; Glowiak, T.; Koll, A. *J. Mol. Struct.* **1999**, *484*, 75.

Scheme 1

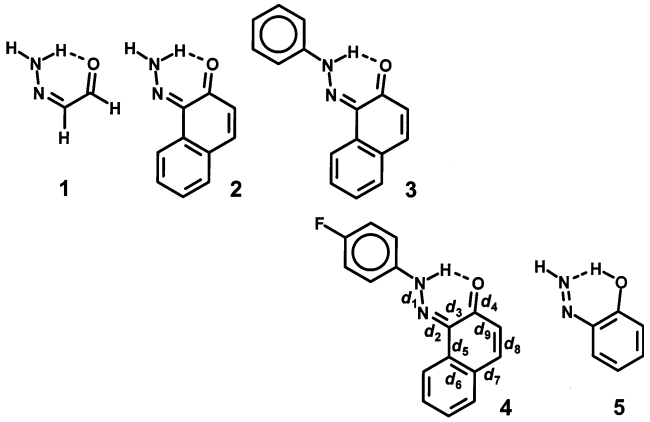

O−H···N have also been reported.[8] On the other hand, solution data show that these compounds undergo fast proton exchange on the NMR time scale between the ketohydrazone and azoenol forms.[8a,9a−d] High-resolution ^{15}N and ^{13}C CP/MAS NMR of solid samples of 1-(aryliminomethyl)- and 1-(arylazo)-2-naphthols indicates equilibrium between N−H···O and O−H···N forms with a $\Delta H°$ of 0.4−0.9 kcal mol^{-1} in favor of the former.[8a,9e,f]

The problem of the N−H···O/O−H···N competition, and in particular of the localization of the H-bond proton, is tackled here in two different and complementary ways: (i) by variable-temperature X-ray crystallographic determination of the structures of two compounds 1-(4-F-phenylazo)2-naphthol (***pF***) and 1-(2-F-phenylazo)2-naphthol (***oF***) that, on the basis of previous literature data[1,6−9] and of a systematic Cambridge Structural Database[10] investigation, were predicted to represent an almost perfect balance between the N−H···O and O−H···N forms; and (ii) by DFT calculations[11] at the B3LYP/6-31+G(d,p)//B3LYP/6-31+G(d,p) level of theory with full geometry optimization and frequency calculation on the ketohydrazone−azoenol series of model molecules **1**−**5** of Scheme 1 in their N−H···O and O−H···N ground states, proton-transfer (PT) transition state (TS), and along their full PT-pathway. This series was chosen as that where the relative stabilities of the ···O=C−C=N−NH··· ketohydrazone and ···HO−C=C−N=N··· azoenol tautomers were expected to change smoothly from weak N−H···O in **1** to strong O−H···N in **5** through very strong N−H···O/O−H···N LBHB in **2**, **3**, and **4**.

Variable-Temperature X-ray Crystallography

It is often reported[3f] that double-minimum X−H···Y bonds are interactions of intermediate strength, at variance with very strong or very weak H-bonds that are more likely to be associated with single-minimum potentials of symmetric or strongly asymmetric nature, respectively. In these intermediate bonds, the PT-barrier is normally low (LBHB[3]) increasing the possibility of solid-state X−H···Y/Y−H···X tautomeric equilibria stabilized by a further entropic contribution of $\Delta G = -RT \ln 2 = -0.41$ kcal mol^{-1}. For β-diketone enols forming intramolecular H-bonds, it has been reported[4b] that the limit between symmetrical single-minimum and double-minimum H-bonds has to be set at d(O···O) ≈ 2.43 Å. A single case of double-minimum O−H···O bond with d(O···O) values of 2.473(3) and 2.532(3) Å (at 147 K) has been extensively investigated by variable-temperature X-ray crystallography. It concerns citrinine, whose proton populations are temperature-dependent in the 20−293 K range and for which an energy difference of 1.6 kcal mol^{-1} between the two minima has been determined[12a] (value successively confirmed by NMR ^{13}C CP/MAS measurements[12b]). Crystallographic studies of intramolecular N−H···O/O−H···N bonds formed by the resonant groups **I**−**III** have sometimes reported the presence of two protons having different occupancies but without attempting any quantitative evaluation.[7a,8a,12c−e] Occupancies were appreciated from bond length changes in the resonant fragment of a thermochromic *N*-salicylideneaniline.[12f] From these data, an energy difference of 0.35(5) kcal mol^{-1} in favor of the N−H minimum can be calculated by van't Hoff analysis, a value which is of the same order of magnitude as that quoted above for 1-arylazo-2-naphthols.[8a]

The crystal structures of ***oF*** and ***pF*** at four temperatures reported in this study represent, therefore, the first attempt at determining the proton occupancies in a low-barrier N···H···O RAHB by full refinement of diffraction data (see Experimental Section). Selected interatomic distances are reported in Table 1, while intramolecular H-bond data, including proton occupancies, are given in Table 2. ORTEP[13] views of the two structures at 100 K are displayed in Figures 1 and 2 (views at the remaining temperatures are available as Figures S1 and S2 of the Supporting Information). Figure 3 reports, for compound ***pF***, the Fourier difference maps at the different temperatures studied computed after full-matrix refinement carried out with the exclusion of the tautomeric proton. They clearly show the progressive decrease of the H(N) and increase of the H(O) occupancies, hereafter indicated as p(NH) and p(OH), occurring with the increase of temperature.

Proton populations p(NH) = 1− p(OH) can be straightforwardly derived from least-squares model refinement of the X-ray data. The results obtained are reported in Table 2. The corresponding parameters for the equilibrium N−H···O ⇄ O−H···N can now be determined (Figure 4) by van't Hoff linear regression $\ln K = \Delta S°/R - \Delta H°/R\ (1/T)$ where the equilibrium constant is $K = p(\mathrm{NH})/p(\mathrm{OH}) = p(\mathrm{NH})/(1 - p(\mathrm{NH}))$. Standard enthalpy values, $\Delta H°$, of −0.120(15) and −0.156(23) kcal mol^{-1} are obtained for ***pF*** and ***oF***, respectively, and can be considered to represent the energy difference between the two N−H···O

(8) (a) Olivieri, A. C.; Wilson R. B.; Paul, I. C.; Curtin, D. Y. *J. Am. Chem. Soc.* **1989**, *111*, 5525. (b) Kurahashi, M. *Bull. Chem. Soc. Jpn*. **1976**, *49*, 2927.
(9) (a) Lyčka, A. *Dyes Pigm.* **1990**, *12*, 179. (b) Lyčka, A.; Jirman, J.; Nečas, M. *Dyes Pigm.* **1991**, *15*, 23. (c) Hansen, P. E.; Bolvig, S.; Buvari-Barcza, A.; Lyčka, A. *Acta Chem. Scand.* **1997**, *51*, 881. (d) Hansen, P. E.; Sitkowski, J.; Rozwadowski, Z.; Dziembowska, T. *Ber. Bunsen-Ges. Phys. Chem.* **1998**, *102*, 410. (e) Benedict, C.; Langer, U.; Limbach, H.-H.; Ogata, H.; Takeda, S. *Ber. Bunsen-Ges. Phys. Chem.* **1998**, *102*, 335. (f) Takeda, S.; Inabe, T.; Benedict, C.; Langer, U.; Limbach, H.-H. *Ber. Bunsen-Ges. Phys. Chem.* **1998**, *102*, 1358.
(10) Allen, F. H.; Bellard, S.; Brice, M. D.; Cartwright, B. A.; Doubleday, A.; Higgs, H.; Hummelink, T.; Hummelink-Peters, B. G.; Kennard, O.; Motherwell, W. D. S.; Rodgers, J.; Watson, D. G. *Acta Crystallogr*. **1979**, *B35*, 2331.
(11) (a) Kohn, W.; Becke, A. D.; Parr, R. G. *J. Phys. Chem.* **1996**, *100*, 12974. (b) Parr, R. G.; Yang, W. *Density Functional Theory of Atoms and Molecules*; Oxford University Press: New York, 1989. (c) Koch, W.; Holthausen, M. C. *A Chemist's Guide to Density Functional Theory*, 2nd ed.; Wiley-VCH: Weinheim, 2001.
(12) (a) Destro, R. *Chem. Phys. Lett.* **1991**, *118*, 232. (b) Poupko, R.; Luz, Z.; Destro, R. *J. Phys. Chem. A* **1997**, *101*, 5097. (c) Inabe, T.; Hoshino, N.; Mitani, T.; Maruyama, Y. *Bull. Chem. Soc. Jpn.* **1989**, *62*, 2245. (d) Inabe, T. *New J. Chem.* **1991**, *15*, 129. (e) Inabe, T.; Luneau, I.; Mitani, T.; Maruyama, Y.; Takeda, S. *Bull. Chem. Soc. Jpn.* **1994**, *67*, 612. (f) Ogawa, K.; Kasahara, Y.; Ohtani, Y.; Harada, J. *J. Am. Chem. Soc.* **1998**, *120*, 7107.
(13) Johnson, C. K. *ORTEPII*; Report ORNL-5138; Oak Ridge National Laboratory: Oak Ridge, TN, 1976.

Table 1. Selected Bond Distances (Å) and π-Delocalization Parameters $\langle\lambda\rangle$ (See Text) for Compounds ***pF*** and ***oF*** at the Four Temperatures Considered (Standard Deviations in Parentheses)

compound	d_1 N_2–N_1	d_2 N_1–C_1	d_3 C_1–C_2	d_4 C_2–O_1	d_5 C_1–C_6	d_6 C_6–C_5	d_7 C_5–C_4	d_8 C_4–C_3	d_9 C_3–C_2	$\langle\lambda\rangle$
pF (100 K)	1.300(2)	1.348(2)	1.450(2)	1.282(2)	1.455(2)	1.415(2)	1.438(2)	1.355(2)	1.439(2)	0.546
pF (150 K)	1.297(2)	1.353(2)	1.440(2)	1.290(2)	1.455(2)	1.415(2)	1.436(2)	1.353(2)	1.434(2)	0.585
pF (200 K)	1.295(2)	1.356(2)	1.437(2)	1.291(2)	1.452(2)	1.415(2)	1.434(2)	1.350(2)	1.434(2)	0.599
pF (295 K)	1.295(2)	1.353(2)	1.433(2)	1.293(2)	1.454(2)	1.413(2)	1.432(3)	1.344(3)	1.426(3)	0.602
oF (100 K)	1.313(2)	1.328(2)	1.460(2)	1.263(2)	1.461(2)	1.411(2)	1.445(2)	1.340(3)	1.452(2)	0.436
oF (150 K)	1.310(2)	1.333(2)	1.453(2)	1.267(2)	1.461(2)	1.410(2)	1.440(3)	1.339(3)	1.447(3)	0.462
oF (200 K)	1.306(2)	1.334(2)	1.452(3)	1.272(3)	1.460(2)	1.415(3)	1.436(3)	1.337(4)	1.443(3)	0.488
oF (295 K)	1.301(3)	1.344(3)	1.447(4)	1.274(3)	1.453(3)	1.410(3)	1.438(4)	1.328(5)	1.439(4)	0.518

Table 2. Intramolecular H-Bond Parameters (Å and Degrees), Tautomeric H-Bond Proton Occupancies for Compounds ***pF*** and ***oF*** at the Four Temperatures Considered, and Thermodynamic Parameters (kcal mol^{-1}) of the O−H···N ⇄ N−H···O Tautomeric Equilibrium (Standard Deviations in Parentheses)

compd	N···O	N–H O–H	H···O N···H	N–H···O N···H–O	p(NH)% p(OH)%	$K = p(NH)/p(OH)$
pF (100 K)	2.535(2)	0.90(3)	1.79(3)	138(3)	64(3)	1.78
		0.94(6)	1.75(5)	139(5)	36(3)	
pF (150 K)	2.533(2)	0.89(3)	1.81(3)	136(3)	60(3)	1.50
		0.96(6)	1.72(5)	141(5)	40(3)	
pF (200 K)	2.532(2)	0.92(3)	1.80(3)	134(3)	58(3)	1.38
		0.92(6)	1.77(5)	139(5)	42(3)	
pF (295 K)	2.536(2)	0.89(4)	1.86(4)	132(4)	54(4)	1.17
		0.96(7)	1.69(6)	144(6)	46(4)	
	$\Delta H° = -0.120(15)$ kcal mol^{-1}; $\Delta S° = 0.0(1)$ cal K^{-1} mol^{-1}					
oF (100 K)	2.546(2)	0.96(2)	1.79(2)	133(2)	77(3)	3.35
		0.97(7)	1.88(8)	123(6)	23(3)	
oF (150 K)	2.543(2)	1.01(3)	1.74(3)	134(2)	75(3)	3.00
		1.02(7)	1.90(8)	117(6)	25(3)	
oF (200 K)	2.540(2)	0.96(3)	1.80(3)	132(2)	73(4)	2.70
		0.97(8)	1.83(8)	128(7)	27(4)	
oF (295 K)	2.540(3)	0.98(3)	1.79(4)	130(3)	69(5)	1.97
		0.99(9)	1.80(9)	129(8)	31(5)	
	$\Delta H° = -0.156(23)$ kcal mol^{-1}; $\Delta S° = 0.7(2)$ cal K^{-1} mol^{-1}					

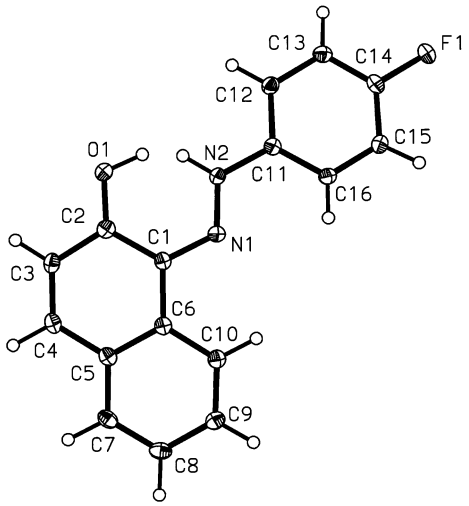

Figure 1. ORTEP[13] view of the molecular structure of compound ***pF*** as determined at 100 K. Thermal ellipsoids are drawn at 40% probability.

and O−H···N ground vibrational levels in a double-minimum potential experienced by the tautomeric proton. The corresponding standard entropy values, $\Delta S°$, are 0.0(1) and 0.7(2) cal K^{-1} mol^{-1}, that is, practically zero as expected in an intramolecular reaction. The reasonable quality of the regressions gives an indirect support to the refinement method presently used (see Experimental Section), though the fact that it makes use only of X-ray diffraction data may suggest to treat with some caution

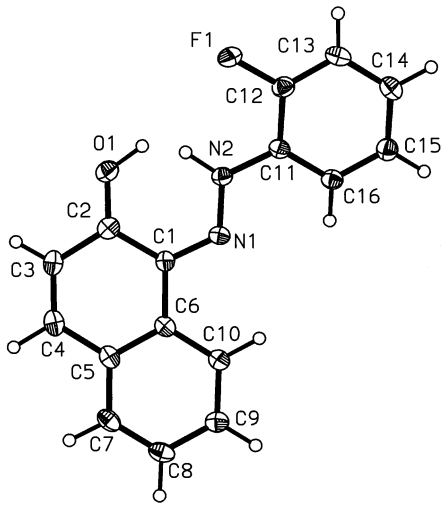

Figure 2. ORTEP[13] view of the molecular structure of compound ***oF*** as determined at 100 K. Thermal ellipsoids are drawn at 40% probability.

the thermodynamic values obtained. Of course, no indication on the height of the PT-barrier, $\Delta^{\ddagger}H$, can be obtained from this treatment, though the substantial linearity of the van't Hoff plots can be taken as a first evidence of a dynamic equilibrium process with high exchange rates at all temperatures and then of very low $\Delta^{\ddagger}H$ values for both compounds. *This classifies the H-bond in* **pF** *and* **oF** *as a true LBHB[3] of the RAHB[4] type with continuous N−H···O/O−H···N exchange even in the solid state.*

DFT Modeling of the Proton-Transfer Process

Computational Methods. DFT modeling of the PT-process for the five test molecules of Scheme 1 has been performed at the B3LYP/6-31+G(d,p)//B3LYP/6-31+G(d,p) level of theory (see Experimental Section for details) by a same strategy, including: (i) full geometry optimization of both N−H···O and O−H···N tautomers in the C_S point group; (ii) identification of the TS of the PT-reaction by the QST2 method;[14] (iii) check of the actual planarity of the molecules in their three stationary points by frequencies evaluation; and (iv) determination of the PT-pathway with full geometry optimization for each of the 23 points of the pathway by the QST3 method.[14] Results are shown in Table 3 and Figures 5−7, while derived AIM properties[15] are illustrated in Figures 8 and 9 and summarized in Table S1 (Supporting Information).

Comparison with Experiments. Direct comparison of experimental and calculated properties is possible only between compound ***pF*** and test molecule **4**. The $\Delta H°$ value derived from

(14) Ayala P. Y.; Schlegel H. B. *J. Chem. Phys.* **1997**, *107*, 375.
(15) Bader, R. F. W. *Atoms in Molecules - A Quantum Theory*; Oxford University Press: Oxford, 1990.

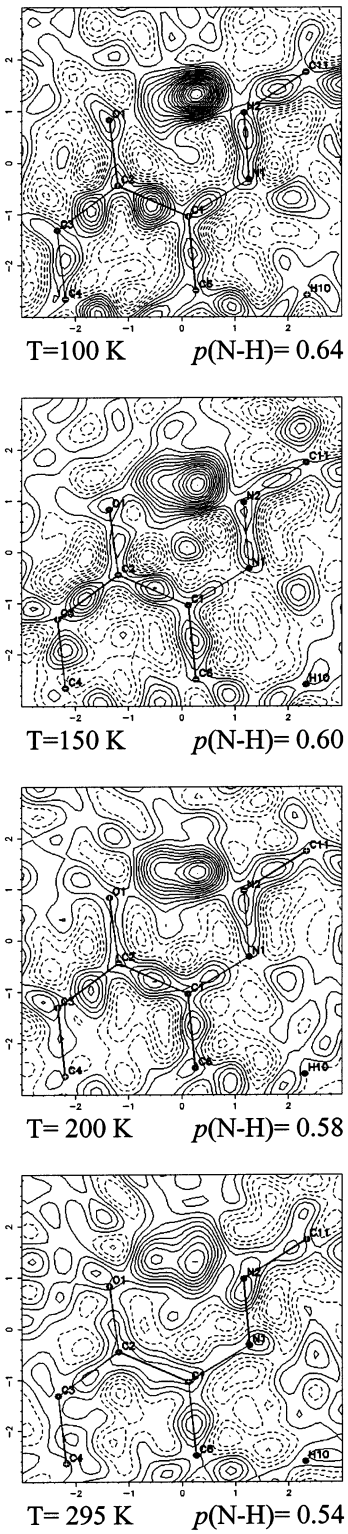

Figure 3. Difference Fourier map in the mean plane of the H-bond chelate ring for compound ***pF*** at the temperatures of 100, 150, 200, and 295 K. Maps were computed after least-squares refinement carried out excluding the H-bond proton. Positive (continuous) and negative (dashed) contours drawn at 0.04 e/Å^3 intervals.

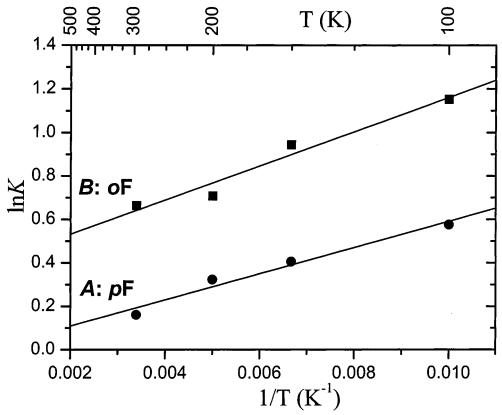

Figure 4. Van't Hoff plots, $\ln K = \Delta S°/R - \Delta H°/R\ (1/T)$, for compounds ***pF*** and ***oF***. $K = p(\mathrm{NH})/p(\mathrm{OH})$ is the ratio of the N−H···O and O−H···N proton populations derived from least-squares refinement. Curve ***A*** (***pF***): $\Delta H° = -0.120(15)$ kcal mol^{-1}, $\Delta S° = 0.0(1)$ cal K^{-1} mol^{-1}, $n = 4$, $r = 0.985$; Curve ***B*** (***oF***): $\Delta H° = -0.156(23)$ kcal mol^{-1}, $\Delta S° = 0.7(2)$ cal K^{-1} mol^{-1}, $n = 4$, $r = 0.980$.

the van't Hoff plot of Figure 4 is −0.120(15) kcal mol^{-1} and compares reasonably well with the thermodynamic values derived from DFT calculations (line ΔX_r(**4**) of Table 3: $\Delta E = -0.403$, $\Delta E^{ZPC} = -0.291$, $\Delta H^{298} = -0.211$, and $\Delta G^{298} = -0.590$ kcal mol^{-1}) out of which ΔE^{ZPC} and ΔH^{298} are probably the most directly comparable with experiments. Table S2 (Supporting Information) compares the X-ray geometry of **4** as determined at 100 K with the DFT-optimized one, evaluated as an average of the N−H···O and O−H···N tautomer geometries weighted according to the corresponding H-bond proton occupancies of 0.64 and 0.36 at 100 K (Table 2). The agreement is good, the average $|\Delta d|$ being 0.006(4) Å for 22 heavy-atom bonds with a maximum $|\Delta d|$ of 0.014 Å. In particular, the experimental and calculated N···O distances are rather similar (2.535(2) and 2.543 Å, respectively) showing that the resonant H-bond is well emulated at the chosen level of theory.

Proton-Transfer Potential-Energy Surface (PT-PES). The energy profile along the PT-pathway as a function of the reaction coordinate $RC = [d(\mathrm{O-H}) - d(\mathrm{N-H})]$ is illustrated in Figure 5 and selected stationary-point properties are given in Table 3. As predicted on the ground of qualitative electrostatic-covalent H-bond model[1,4c] considerations, the PES is strongly asymmetric in favor of the N−H···O form for **1**, becomes increasingly symmetric for **2**, **3**, and **4**, and is reversed for **5** where the O−H···N form becomes preferred. The ΔX values (X = E, E^{ZPC}, H^{298}, G^{298}) reported in Table 3 have the meaning of the negative of activation energies for the PT-process, $-\Delta^{\ddagger}X$, while the energy differences between the two minima, ΔX_r, that of reaction energies. The whole of data indicates that the decrease of ΔX_r (i.e., the symmetrization of the PT-PES) is associated with a decrease (increase) of $\Delta^{\ddagger}X$ for the more (less) stable H-bond and with a shortening (lengthening) of the distance between the minimum and the TS along the reaction coordinate, $\Delta^{\ddagger}d$, according to the Hammond postulate.[16a] However, all activation energies become remarkably smaller, and sometimes fade, when molecular vibrations are taken into account, as shown in Figure 5 by the small horizontal lines drawn above the two minima and marking the relative energies corrected for zero-point vibrational contributions (ΔE^{ZPC}).

(16) (a) Hammond, G. S. *J. Am. Chem. Soc.* **1955**, *77*, 334. (b) Marcus, R. A. *Discuss. Faraday Soc.* **1960**, *29*, 21. (c) Marcus, R. A. *J. Phys. Chem.* **1968**, *72*, 891. (d) Murdoch, J. R. *J. Am. Chem. Soc.* **1972**, *94*, 4410. (e) More O'Ferral, R. A. *J. Chem. Soc. B* **1970**, 274. (f) Grunwald, E. *J. Am. Chem. Soc.* **1985**, *107*, 125. *(g)* Shaik, S. S.; Schlegel, H. B.; Wolfe, S. *Theoretical Aspects of Physical Organic Chemistry. The S_N2 Mechanism*; John Wiley: New York, 1992. (h) Wolfe, S.; Mitchell, D. J.; Schlegel, H. B. *J. Am. Chem. Soc.* **1981**, *103*, 7694.

Table 3. Stationary-Point DFT-Calculated Energies Relative to TS Chosen as Zero, ΔX ($X = E$, E^{ZPC}, H^{298}, G^{298}), Distances from TS along the Reaction Coordinate RC = [d((O−H) − d(N−H)], $\Delta^{\ddagger}d$, Selected Distances and Angles, π-Delocalization Parameters $\langle\lambda\rangle$ (See Text), and Pauling's Bond Numbers[18a] of the N−H and O−H Bonds, n(OH) and n(NH), for the Test Molecules **1**−**5** of Scheme 1[a]

test molecule	ΔE	ΔE^{ZPC}	ΔH^{298}	ΔG^{298}	$\Delta^{\ddagger}d$	N···O	N–H	H···O	N–H–O	RC	d_1 N–N	d_2 N=C	d_3 C–C	d_4 C=O	$\langle\lambda\rangle$	n(NH)	n(OH)
1 NH···O	−10.76	−8.51	−7. 99	−8.93	1.106	2.674	1.021	1.914	128.7	0.893	1.313	1.313	1.449	1.238	0.319	0.927	0.073
1 TS	0	0	0	0	0	2.395	1.349	1.136	148.8	−0.213	1.286	1.365	1.389	1.297	0.635	0.396	0.593
1 OH···N	−0.68	1.53	1.78	1.31	0.384	2.517	1.618	1.021	144.1	−0.597	1.275	1.383	1.372	1.319	0.740	0.197	0.808
ΔX_r(**1**)	−10.08	−10.04	−9.77	−10.24													
2 NH···O	−4.87	−2.36	−1.97	−2.75	0.780	2.566	1.029	1.760	132.1	0.731	1.306	1.325	1.476	1.256	0.417	0.908	0.110
2 TS	0	0	0	0	0	2.374	1.255	1.206	149.5	−0.049	1.287	1.361	1.437	1.300	0.645	0.505	0.491
2 OH···N	−2.48	0.00	0.22	−0.15	0.582	2.526	1.638	1.007	144.4	−0.631	1.271	1.389	1.414	1.334	0.799	0.186	0.839
ΔX_r(**2**)	−2.39	−2.36	−2.19	−2.60													
3 NH···O	−3.69	−0.99	−0.73	−1.39	0.699	2.555	1.038	1.695	137.1	0.657	1.307	1.330	1.474	1.260	0.436	0.887	0.131
3 TS	0	0	0	0	0	2.386	1.253	1.211	150.9	−0.042	1.292	1.360	1.438	1.301	0.633	0.508	0.484
3 OH···N	−2.58	−0.11	0.10	−0.45	0.590	2.535	1.640	1.008	145.4	−0.632	1.276	1.384	1.416	1.336	0.783	0.186	0.837
ΔX_r(**3**)	−1.11	−0.88	−0.83	−0.94													
4 NH···O	−3.33	−0.65	−0.39	−1.03	0.670	2.546	1.039	1.681	137.5	0.642	1.307	1.330	1.474	1.260	0.436	0.885	0.136
4 TS	0	0	0	0	0	2.384	1.246	1.218	150.9	−0.028	1.292	1.360	1.439	1.300	0.630	0.514	0.475
4 OH···N	−2.93	−0.36	−0.18	−0.44	0.612	2.538	1.646	1.006	145.3	−0.640	1.276	1.384	1.416	1.336	0.783	0.183	0.842
ΔX_r(**4**)	−0.40	−0.29	−0.21	−0.59													
5 NH···O	−2.57	−0.23	0.12	−0.52	0.627	2.554	1.036	1.714	135.0	0.678	1.300	1.336	1.478	1.261	0.452	0.892	0.125
5 TS	0	0	0	0	0	2.383	1.210	1.261	149.4	0.051	1.284	1.366	1.449	1.298	0.641	0.568	0.423
5 OH···N	−4.91	−2.29	−2.04	−2.49	0.761	2.575	1.707	0.997	143.2	−0.710	1.265	1.400	1.426	1.341	0.832	0.156	0.862
ΔX_r(**5**)	2.34	2.06	2.16	1.97													
$\Delta^{\ddagger}X_o$	3.130	0.495	0.274	0.704													

[a] The last line reports the heights of the intrinsic barriers, $\Delta^{\ddagger}X_o$, calculated according to the Marcus theory[16] from the corresponding thermodynamic value $\Delta X_r = \Delta X$(N−H···O) − ΔX(O−H···N). Energies in kcal mol^{-1}, distances in Å, and angles in degrees.

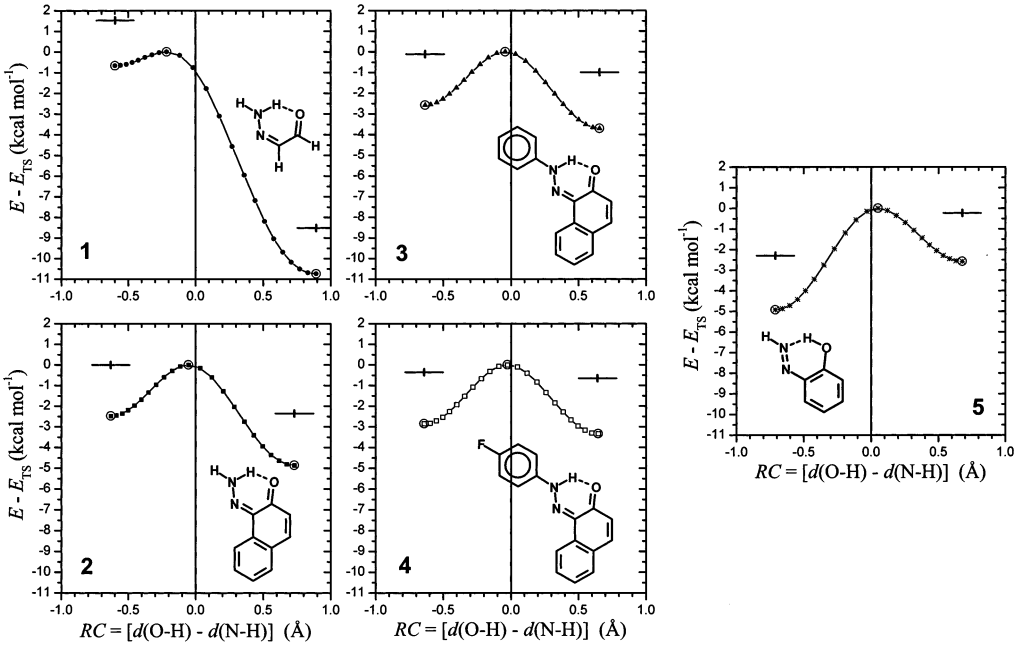

Figure 5. Relative energies in kcal mol^{-1}, ΔE, referred to the TS taken as zero and plotted along the proton-transfer reaction coordinate RC = [d(O−H) − d(N−H)] (Å) as calculated by DFT methods for test molecules **1**−**5** of Scheme 1. The short horizontal lines marked above the minima indicate the relative energies corrected for the zero-point vibrational contribution, ΔE^{ZPC}. DFT-optimized stationary points are marked by encircled symbols.

Relationships between ΔX_r and $\Delta^{\ddagger}X$ are better seen in the frame of the semiempirical Marcus rate-equilibrium theory[16b−h] according to which

$$\Delta^{\ddagger}X_i = \Delta^{\ddagger}X_o + \Delta X_{r,i}/2 + (\Delta X_{r,i})^2/(16\,\Delta^{\ddagger}X_o) \qquad (1)$$

where $\Delta X_{r,i}$ and $\Delta^{\ddagger}X_i$ are the reaction and activation energies for the ith reaction and $\Delta^{\ddagger}X_o$ is the intrinsic barrier (also called γ), that is, the formal PT-barrier occurring in the symmetric case for which $\Delta X_r = 0$. Equation 1 allows us to calculate $\Delta^{\ddagger}X_o$ values by simple recursive methods as well as new values of $\Delta^{\ddagger}X_i = f(\Delta X_{r,i})$ (that can be called "Marcus $\Delta^{\ddagger}X$") to be compared with the "DFT-calculated $\Delta^{\ddagger}X$" of Table 3. Figure S3 (Supporting Information) shows that the comparison of these two quantities gives a straight line having nearly unitary slope, so confirming the validity of the Marcus model for the PT-reaction in this class of compounds.

The last row of Table 3 reports the calculated values of $\Delta^{\ddagger}X_o$, which are $\Delta^{\ddagger}E_o = 3.130$, $\Delta^{\ddagger}E_o^{ZCP} = 0.495$, $\Delta^{\ddagger}H_o^{298} = 0.274$, and $\Delta^{\ddagger}G_o^{298} = 0.704$ kcal mol^{-1}, out of which the most realistic

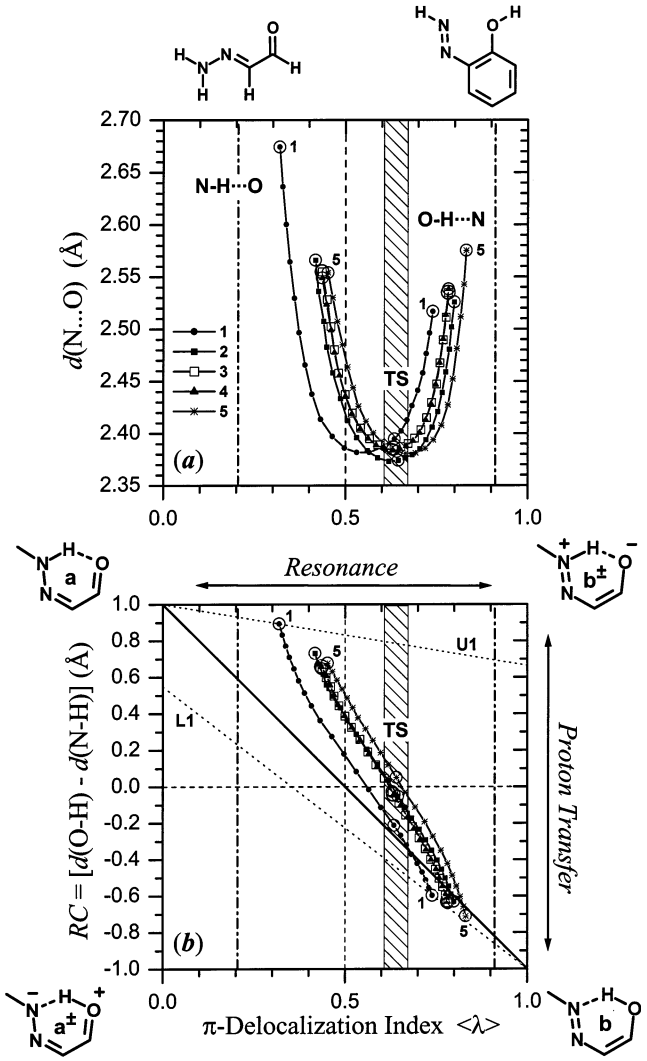

Figure 6. (a) N···O contact distances and (b) reaction coordinate $RC = [d(\mathrm{O-H}) - d(\mathrm{N-H})]$ (Å) plotted against the π-delocalization index $\langle\lambda\rangle$ as calculated by DFT methods along the PT-pathway for test molecules **1**−**5** of Scheme 1. DFT-optimized stationary points are marked by encircled symbols.

might be $\Delta^{\ddagger}E_o^{ZCP}$ because $\Delta^{\ddagger}E_o$ is lacking a clear physical meaning and room-temperature vibrational analysis has been performed in a harmonic approximation despite the softness of the H-bond potential. It can be concluded that a value of 0.5 kcal mol^{-1} sets the lowest limit to the PT-barrier, occurring when the substituents are chosen in such a way that the two N−H···O and O−H···N tautomers are isoenergetic ($\Delta X_r = 0$). In other words, *this particular resonant system does not seem able to form single-minimum H-bonds but only LBHBs irrespectively of chemical substitution.*

Geometrical Structure Correlations along the DFT-Modeled PT-Pathway

Importance of π-Delocalization in N−H···O/O−H···N RAHB. Intercorrelations among geometrical parameters (structure correlations[17]) are of particular interest for RAHB because of the synergistic interplay between H-bond strengthening and increasing delocalization of the π-conjugated fragment connecting the H-bond donor and acceptor groups that occurs in this class of bonds.[4] Such structure correlations can be easily derived from the complete set of DFT-molecular geometries

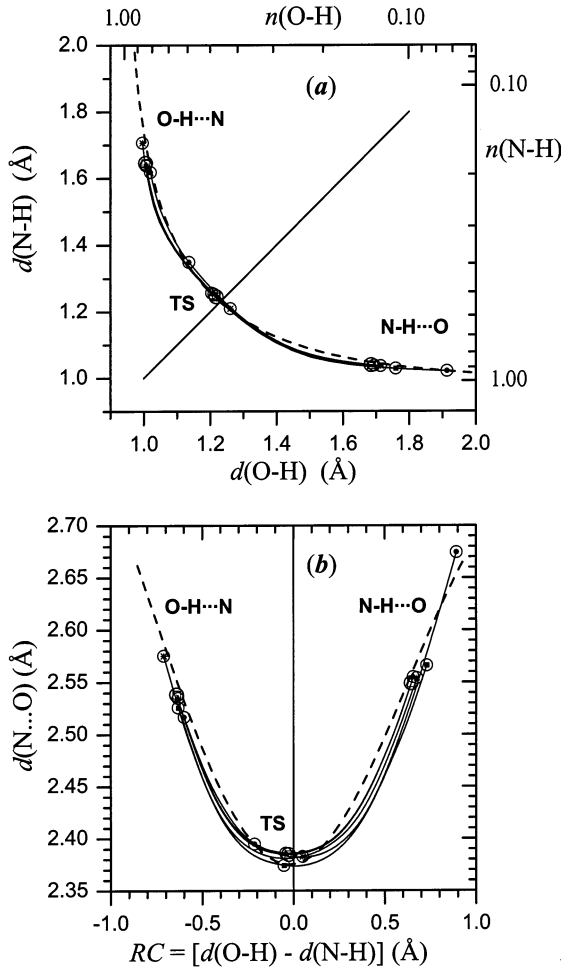

Figure 7. (a) N−H bond distances plotted against the O−H ones (Å), and (b) N···O contact distances plotted against the reaction coordinate $RC = [d(\mathrm{O-H}) - d(\mathrm{N-H})]$ (Å) as calculated by DFT methods along the PT-pathway for test molecules **1**−**5** of Scheme 1. DFT-optimized stationary points are marked by encircled symbols. The dashed curves map the structure correlations derived from neutron crystallography[20b] according to eq 4 in a and eq 6 in b.

obtained by QST3 for each point of the PT-pathway connecting the three stationary points. Selected geometrical parameters are collected in Table 3 and some relevant structure correlations among them are displayed in Figures 6 and 7.

In RAHB systems, the proton transfer from N−H···O to O−H···N is associated with the exchange of the single and double bonds within the resonant fragment, as illustrated in **VII**, causing bond changes (Table 3) where the decrease of d_1 and d_3 is paralleled by the increase of d_2 and d_4. It is then possible to monitor the progress along the reaction coordinate through an essentially geometrical index of π-delocalization based on the four d_1-d_4 or, in case, on the nine d_1-d_9 distances[1b] transformed into bond numbers, n, through the Pauling equation[18a−c] $d(n) = d(1) - c \log_{10} n$, where $d(n)$ and $d(1)$ are the bond lengths for the bond numbers n and 1, respectively,

(17) (a) Bent, H. A. *Chem. Rev.* **1968**, *68*, 587. (b) Bürgi, H.-B. *Inorg. Chem.* **1973**, *12*, 2321. (c) Bürgi, H.-B.; Dunitz, J. D.; Shefter, E. *J. Am. Chem. Soc.* **1973**, *95*, 5065. (d) Murray-Rust, P.; Bürgi, H.-B.; Dunitz, J. D. *J. Am. Chem. Soc.* **1975**, *97*, 921. (e) Bürgi, H.-B.; Dunitz, J. D. *Acc. Chem. Res.* **1983**, *16*, 253. (f) Dunitz, J. D. *X-ray Analysis and the Structure of Organic Molecules*; Cornell University Press: Ithaca, NY, 1979. (g) *Structure Correlations*; Bürgi, H.-B., Dunitz, J. D., Eds.; VCH: Weinheim, 1994. (h) Ferretti, V.; Gilli, P.; Bertolasi, V.; Gilli, G. *Cryst. Rev.* **1996**, *5*, 3−104.

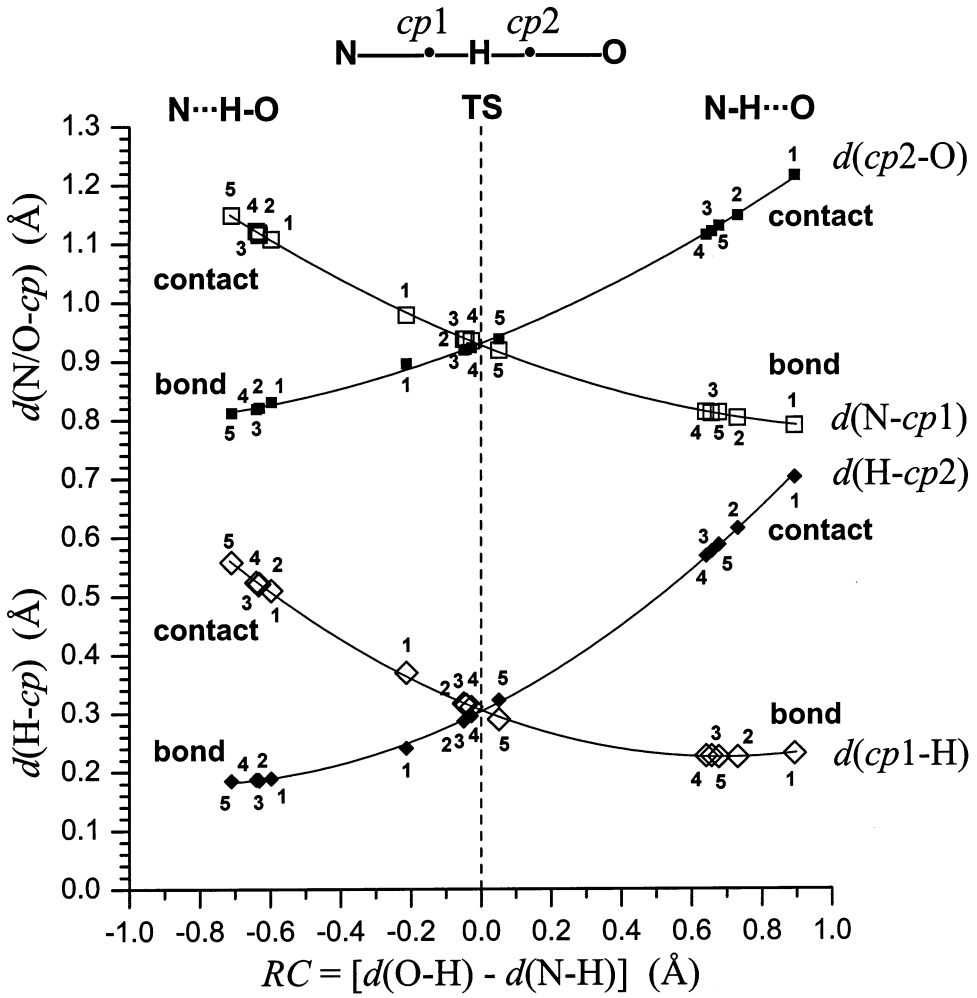

Figure 8. H-bond critical-point distances. N-*cp*1 and *cp*2-O (upper diagram) and *cp*1-H and H-*cp*2 (lower diagram) distances (Å) plotted against the reaction coordinate $RC = [d(\mathrm{O-H}) - d(\mathrm{N-H})]$ (Å) as calculated by AIM analysis[15] of DFT-optimized stationary points for test molecules **1**−**5** of Scheme 1. Interpolating continuous lines have purely graphical purposes.

and c is a constant to be evaluated. An average index of π-delocalization, $\langle\lambda\rangle$, can then be calculated,[18d] which assumes the values of 0, 1, and 0.5 for the ketohydrazonic **VIIa**, azoenolic **VIIb**, and completely π-delocalized mixed forms, respectively. Stationary-point computed values of $\langle\lambda\rangle$ are reported in Table 3 and can be compared with the experimental ones for ***pF*** and ***oF*** given in Table 1.

As expected for RAHB, the variations of $\langle\lambda\rangle$ with *RC* (Figure 6b) are remarkably wide, ranging from 0.32 to 0.83. It seems of interest that the proton transfer at TS does not occur at $\langle\lambda\rangle = 0.5$ (as would be expected for homonuclear X−H···X RAHB) but is shifted toward the enolimino form in the restricted range of $\langle\lambda\rangle = 0.637 \pm 0.005$ indicated in Figure 6 by the vertical shadowed bands. This could well be a general feature of all N−H···O/O−H···N heteronuclear bonds in relation with the fact that the two tautomeric ketohydrazone forms are differently delocalized also in their non-H-bonded ground states sketched on the top of Figure 6 and indicated by the two vertical dash−dot lines located at $\langle\lambda\rangle = 0.205$ and 0.911, respectively.

Figure 6a monitors the parallel dramatic decrease of the N···O distance while the system approaches TS, which appears to be nearly invariantly located, for all molecules investigated, in a strict interval not only of $\langle\lambda\rangle$ but also of N···O distances (2.384 ± 0.007 Å) and N−H−O angles (150 ± 1°). On the contrary, the two N−H···O and O−H···N ground states take place at much longer N···O distances and weaker delocalizations of the π-conjugated system, the displacements from TS being the larger the greater the energy difference with TS is (Table 3 and Figure 5). This fact, that essentially expresses the Hammond postulate,[16a] leads to the rule that *the less stable H-bond is always stronger (shorter) than the more stable one*, a difference that fades only with the PT−PES symmetrization.[19]

A Simplified VB Theory of N−H···O/O−H···N RAHB. Present findings can be easily rationalized in terms of simplified VB theory by representing each of the two N−H···O and

(18) (a) Pauling, L. *J. Am. Chem. Soc.* **1947**, *69*, 542. (b) Pauling, L. *The Nature of the Chemical Bond*, 3rd ed.; Cornell University Press: Ithaca, NY, 1960. (c) Bürgi, H.-B.; Dunitz, J. D. *J. Am. Chem. Soc.* **1987**, *109*, 2924. (d) Values for pure single- and double-bond distances used in the calculations are (1.49−1.33), (1.38−1.20), (1.41−1.27), and (1.39−1.24) Å for $C(sp^2)-C(sp^2)$, $C(sp^2)-O$, $C(sp^2)-N(sp^2)$, and $N(sp^2)-N(sp^2)$ bonds, respectively. The average index of π-delocalization $\langle\lambda\rangle$ is calculated[1b] as $\langle\lambda\rangle = \Sigma_i = {}^4_1\lambda_i/4$ with $\lambda_1 = n_1 - 1$, $\lambda_2 = 2 - n_2$, $\lambda_4 = 2 - n_4$, and $\lambda_3 = n_3 - 1$ for simple ketohydrazones **V**, or $\lambda_3 = 1/2\,[n_3 + \Sigma_{i=}{}^9_5\lambda_i/5] - 1$ when the ketohydrazone is fused with an aromatic ring (**VI** and **VII**).

(19) This statement can be quantitatively verified by computing the H-bond energy, E_{HB}. Its values can be easily estimated for the O−H···N form from the difference between the total energy of the "H-bonded molecule" and that of its "open form" obtained by 180° rotation of the O−H bond around the phenolic C−O bond (d_4). E_{HB} values so obtained are 15.108, 15.039, 14.643, 14.248, and 13.095 kcal mol^{-1} for test molecules **1**−**5**, respectively, and apparently they are continuously decreasing while the thermodynamic stability of the corresponding O−H···N bonds is increasing (Figure 5).

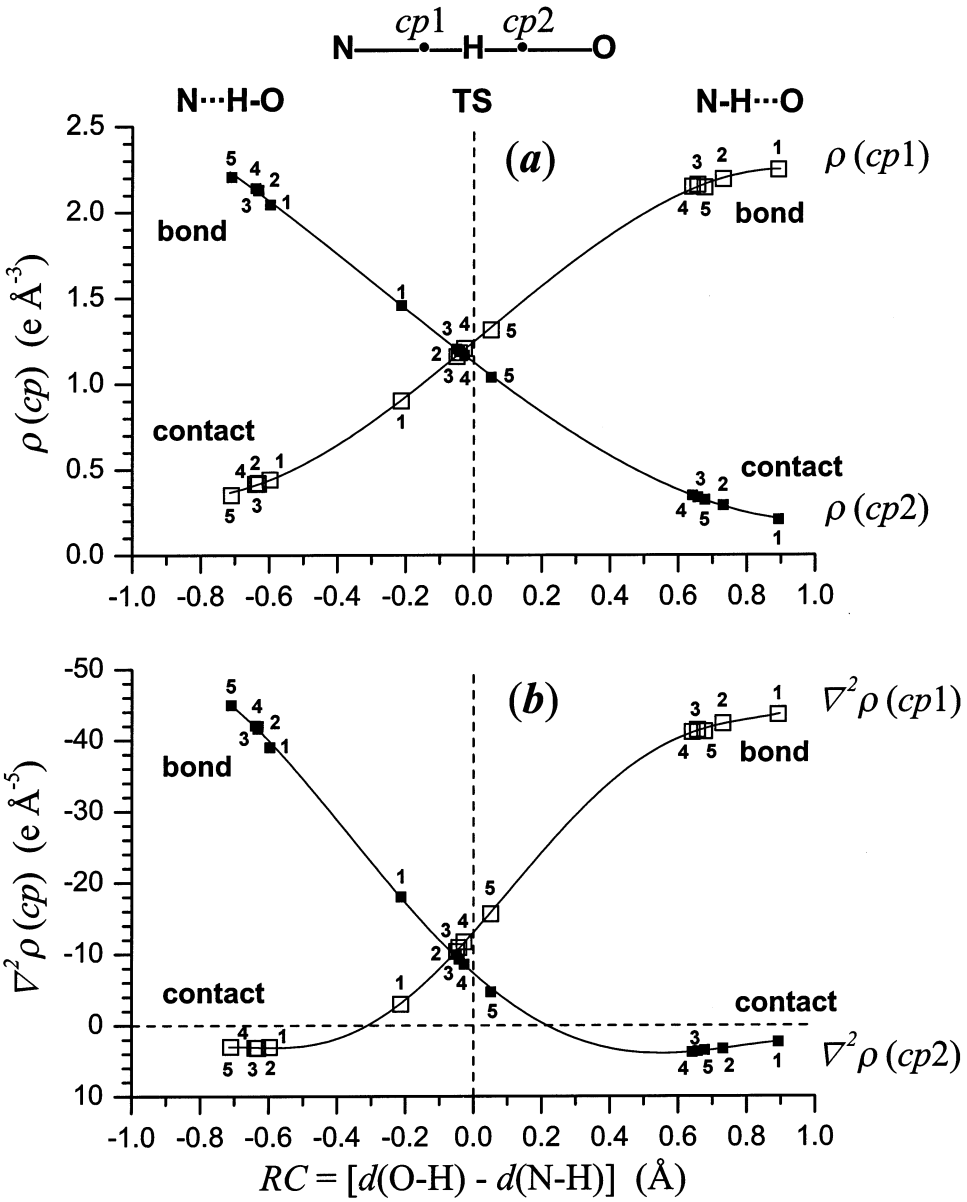

Figure 9. H-bond critical-point parameters. (a) $\rho(cp)$ (eÅ^{-3}) and (b) $\nabla^2\rho(cp)$ (eÅ^{-5}) plotted against the reaction coordinate $RC = [d(\mathrm{O-H}) - d(\mathrm{N-H})]$ (Å) as calculated by AIM analysis[15] of DFT-optimized stationary points for test molecules **1**−**5** of Scheme 1. Interpolating continuous lines have purely graphical purposes.

O−H···N tautomers (**a** and **b** in **V**−**VII**) as a mixture of the four VB resonance forms drawn at the corners of Figure 6b, two of which neutral (**a** and **b**) and two ionic ($\mathbf{a}^{\pm}$ and $\mathbf{b}^{\pm}$), according to the following combinations of VB wave functions

$$\Psi(\mathrm{N-H\cdots O}) = \mathrm{a}\,\Psi(\mathbf{a}) + \mathrm{b}\,\Psi(\mathbf{b}) + \mathbf{b}^{\pm}\,\Psi(\mathbf{b}^{\pm}) \quad (2)$$

$$\Psi(\mathrm{O-H\cdots N}) = \mathrm{b}\,\Psi(\mathbf{b}) + \mathrm{a}\,\Psi(\mathbf{a}) + \mathbf{a}^{\pm}\,\Psi(\mathbf{a}^{\pm}) \quad (3)$$

This method was introduced in our first paper dedicated to O−H···O RAHB[4a] and can now be applied to the interpretation of the N−H···O/O−H···N bond as well. The localization of any actual geometry within the upper-right (**abb**$^{\pm}$) and lower-left (**baa**$^{\pm}$) triangles of Figure 6b gives, in fact, an appreciation of the three coefficients to be applied in eqs 2 and 3. The upper horizontal axis **a**−$\mathbf{b}^{\pm}$ (right-oriented) is a measure of the mixing of **a** and $\mathbf{b}^{\pm}$, and the lower one **b**−$\mathbf{a}^{\pm}$ (left-oriented) is a measure of the mixing of **b** and $\mathbf{a}^{\pm}$ in a N−H···O and O−H···N bond, respectively, which is purely electrostatic in nature and occurs without any N−H or O−H bond lengthening. On the other hand, the main diagonal connecting **a** and **b** is a line of annihilation of charges because of the equal contributions of the polar forms $\mathbf{a}^{\pm}$ and $\mathbf{b}^{\pm}$ and represents the locus of points of the covalent N···H···O bond which is just a mixture of the neutral **a** and **b** forms.

From a purely qualitative point of view, Figure 6b admits a quite simple interpretation. Strong homonuclear O−H···O RAHBs occurring in β-diketone enols are double-minimum or low-barrier H-bonds where the representative points of the equivalent O−H···O and O···H−O forms are symmetrically arranged on the two half-diagonals and separated by a small energy barrier having the TS at the exact center of the plot. In very strong O−H···O bonds of this sort, the barrier disappears (or better becomes smaller than the zero vibrational level of the proton) forming a single-minimum or no-barrier H-bond

Table 4. Mixing Coefficients (×100) in Eqs 2 and 3 of the Four Canonical Forms **a**, **b**, $\mathbf{a}^{\pm}$, and $\mathbf{b}^{\pm}$ Displayed at the Corners of Figure 6b (NHB−KH and NHB−AE Are the Non-H-Bonded Ketohydrazone and Azoenol Forms Shown on the Top of Figure 6a, Respectively)

test molecule	**a** (×100)	**b** (×100)	$\mathbf{a}^{\pm}$ (×100)	$\mathbf{b}^{\pm}$ (×100)
NHB−KH	79.5	0.0		20.5
1 N−H···O	68.1	5.4		26.6
2 N−H···O	58.3	13.4		28.3
3 N−H···O	56.4	17.1		26.4
4 N−H···O	56.4	17.7		25.9
5 N−H···O	54.8	16.1		29.1
1 TS	36.5	60.6		2.9
2 TS	35.5	52.6		11.9
3 TS	36.6	52.1		11.2
4 TS	37.0	51.3		11.7
5 TS	35.9	47.4		16.7
1 O−H···N	20.1	74.0	5.9	
2 O−H···N	18.5	79.9	1.7	
3 O−H···N	18.4	78.3	3.3	
4 O−H···N	18.0	78.3	3.7	
5 O−H···N	14.5	83.2	2.4	
NHB−AE	0.0	91.1	8.9	

localized at or very near the center of the plot, which is a 1:1 mixture of the two neutral **a** and **b** forms and, for this reason, has been classified as a true three-center-four-electron covalent bond.[4c] In N−H···O/O−H···N heteronuclear RAHBs, the very strong symmetric N···H···O bond cannot be achieved even when the different PAs of the N and O atoms are equalized by a proper choice of substituents, most probably because of the insufficient electronegativity of the N atom.[20a] Accordingly, even the strongest RAHBs can only be LBHBs where the two N−H···O and O−H···N tautomers are still separated by a small PT-barrier whose TS does not need to be at the center of the plot because of the heteronuclear nature of the bond.

Stationary-point coefficients in eqs 2 and 3 can be appreciated by applying a kind of lever rule[21] to the upper and lower triangles of Figure 6b. Final results are summarized in Table 4.

Covalent or Electrostatic Nature of N−H···O/O−H···N RAHB. H-bond strengthening occurring in N−H···O/O−H···N RAHBs has been variously attributed to **a**−**b** covalent[1,6] or **a**−$\mathbf{b}^{\pm}$ (or **b**−$\mathbf{a}^{\pm}$) ionic mixing[7] of VB resonance forms. Figure 6b and the mixing coefficients of Table 4 can now be used to provide us a better understanding of the problem. Molecule **1** can be considered to be the epitome of a "normal" N−H···O RAHB endowed by strongly dissymmetric PT-PES (Figure 5-**1**). In this case, the stable N-H···O bond is mostly electrostatic (**b**:$\mathbf{b}^{\pm}$ = 5:27) while TS is covalent (**b**:$\mathbf{b}^{\pm}$ = 61:3), as it would essentially be the unattainable O−H···N form (**a**:$\mathbf{a}^{\pm}$ = 20:6). Symmetrization of the PT-barrier in **2**−**5** gives rather similar TSs having a nearly 51:13 ratio of covalency to ionicity. At the same time, the two tautomers become more symmetrically disposed around the TS itself but maintain very different bonding properties: the N−H···O bond slightly increases its covalent character up to a covalent:ionic ratio of 16:27 while the O−H···N one remains essentially covalent in all cases, its ratio being 17:3 on average. This discussion seems to lead to two interesting implications on the nature of N−H···O/O−H···N RAHBs: (i) the TS H-bond is essentially covalent in all instances; (ii) the O−H···N bond has always a much more covalent character than the prevalently ionic N−H···O one.

Comparison of DFT-Modeled and Crystallographic Structure Correlations. The idea that structure correlations among the internal geometrical variables of a molecular fragment do follow minimum energy pathways in the fragment PES and that their extrapolation can be used to get correct TS geometries has been sometimes called "structure-correlation principle".[17d−f] When verified, it establishes a useful relationship between X-ray and neutron crystallography and chemical kinetics.

PT-processes in X−H···Y bonds can be studied by structure-correlation methods because the form of the d(Y−H) = f[d(X−H)] function is known, being empirically derivable by a combination of the Pauling equation[18a] (see above) with the bond-number conservation rule[17] for three-center-four-electron systems, n(X−H) + n(Y−H) = 1. For the N−H···O bond, the final equation is

$$d(\mathrm{N-H}) = d^{\circ}(\mathrm{N-H}) - c(\mathrm{N-H}) \log_{10}\{1 - 10^{[d^{\circ}(\mathrm{O-H}) - d(\mathrm{O-H})]/c(\mathrm{O-H})}\} \quad (4)$$

where d(N−H) and d(O−H) are the actual H-bond distances and $d°$(N−H) and $d°$(O−H) are the same distances in the absence of the H-bond. Coefficients $d°$(N−H) = 0.992, $d°$(O−H) = 0.942, c(N−H) = 0.887, and c(O−H) = 0.854 Å have been recently determined[20b] from the high-precision low-temperature neutron structures of 49 molecules forming intermolecular N−H···O/O−H···N bonds of different strengths though all very far from the TS geometry.

Figure 7a,b shows, as continuous lines, the variations of d(N−H) versus d(O−H) and d(N···O) versus *RC* along the DFT-calculated PT-pathways of test molecules **1**−**5** of Scheme 1. The five curves have very similar shapes, differing mostly for the ground-state and TS positions. The dashed line of Figure 7a has been drawn according to eq 4 using the constants given above[20b] and is seen to approximate quite well the DFT-calculated pathway also in the TS region that was completely unaccessible to neutron diffraction experiments. This seems a first indication in favor of the reliability of the structure-correlation principle when applied to PT-processes, a result even more significant when considering that coefficients of eq 4 were determined for essentially linear intermolecular H-bonds and we are now using them for intramolecular RAHBs with remarkably bent N−H−O angles (Table 3). This would indicate that the N···H···O bond can be really treated, at least at a first approximation, as a three-center interaction whose independent variables are the N−H and O−H distances, irrespectively of the range of N−H−O angular values.

Less easy is to account for the shape of the d(N···O) versus *RC* plot of Figure 7b because the N−H−O angles assume rather

(20) (a) No example of single-minimum or no-barrier H-bond of N−H···O/O−H···N RAHB type has so far been discovered. However, such a N···H···O bond was recently found in another class of strong heteronuclear H-bonds, that of (±)CAHB with close pK_a matching. It concerns the intermolecular acid−base complex between pentachlorophenol and 4-methylpyridine for which a nearly symmetric bond with d(N···O) = 2.513(3) Å was measured by neutron diffraction at 100 K by (a) Steiner, Th.; Majers, I.; Wilson, C. C. *Angew. Chem., Int. Ed.* **2001**, *40*, 2651. (b) Steiner, Th. *J. Phys. Chem.* **1998**, *102*, 7041.

(21) With reference to Figure 6b, geometries on the dotted line **U1** share the same b/$b^{\pm}$ ratio of ≃ 17/83, which is the inverse ratio of the two segments cut by **U1** on the **b**-$\mathbf{b}^{\pm}$ vertical axis. The N−H···O bond in **1** cuts, moreover, a ratio a/(b + $b^{\pm}$) of ≃ 68/32 on the top **a**−$\mathbf{b}^{\pm}$ horizontal axis, which leads to the final values a = 0.68, b = 0.05, and $b^{\pm}$ = 0.27. In a similar way, the ratio a/$a^{\pm}$ ≃ 77/23 cut by the dotted line **L1** on the **a**-$\mathbf{a}^{\pm}$ vertical axis combined with the ratio b/(a + $a^{\pm}$) ≃ 74/26 cut on the bottom horizontal axis **b**−$\mathbf{a}^{\pm}$ gives the final values of a = 0.20, b = 0.74, and $a^{\pm}$ = 0.06. Application of this simple method to all stationary-point geometries of Table 3 leads to the final results summarized in Table 4.

different values for the three stationary points, being 129−138°, 143−145°, and 149−151° for N−H···O, O−H···N, and TS, respectively (Table 3). Angles, however, change only smoothly with *RC* and in a strictly similar manner for all compounds **1**−**5** (see Figure S4 of Supporting Information) so that they can be fitted by the regression equation

$$\alpha(\mathrm{N{-}H{-}O}) = 150.0(1) - 6.1(2)\,RC - 22.4(5)\,(RC)^2 \quad (5)$$
$$(n = 115,\ r = 0.986,\ \alpha \text{ in degrees})$$

by which d(N···O) values can be calculated for any d(N−H)/d(O−H) pair along *RC* making proper allowance for the corresponding α(N−H−O) value, that is,

$$d(\mathrm{N\cdots O}) = [d(\mathrm{N{-}H})^2 + d(\mathrm{O{-}H})^2 - 2\,d(\mathrm{N{-}H})\,d(\mathrm{O{-}H})\cos\alpha(\mathrm{N{-}H{-}O})]^{1/2} \quad (6)$$

The d(N−H) versus d(O−H) curve of eq 4 can be transformed into the corresponding d(N···O) versus *RC* curve shown by the dashed line of Figure 7b. The fitting with the average DFT-calculated pathway is still remarkable and can be taken as a further indication that *crystal structure correlations do actually map low-energy pathways on the PES of the PT reaction*.

AIM Analysis along the DFT-Modeled PT-Pathway

Since H-bond is normally found to link strongly electronegative atoms, it has been considered a mostly ionic or electrostatic interaction from the very beginning.[18b] However, the evidence that covalent forces cannot be neglected in very strong H-bonds has been considered from time to time,[22] finally leading to the assessment that very strong homonuclear O−H···O bonds are actually three-center-four-electron covalent bonds.[4c] However, the assessment of H-bond covalency turned out to be a rather tricky matter until the introduction of AIM methods[15] of topological analysis of the experimental or calculated electron densities. It is now generally recognized that H-bonds can be classified as mostly covalent (shared interactions) or mostly electrostatic (closed-shell interactions) according to whether the H-bond (3,−1) critical point (*cp*) has negative or positive Laplacian ($\nabla^2\rho(cp) < 0$ or $\nabla^2\rho(cp) > 0$, respectively) while the electron density at the H-bond critical point, $\rho(cp)$, increases with the degree of covalency. Association of these methods with combined X-ray and neutron diffraction electron-density measurements has attested the evidence of negative Laplacians (and then of covalency) in a few strong O−H···O bonds of charge-assisted[23a−c] and resonance-assisted[23d,e] type, though the reliability of second derivatives of experimental densities must always be considered with some caution.[23f]

Covalency is not expected to dominate heteronuclear N−H···O/O−H···N RAHBs, in particular of the double-minimum type. AIM methods, however, can still be of great help in the present case for assessing the variations in chemical-bond nature occurring along the PT-pathway. Present results are illustrated in Figures 8 and 9 and Table S1 (Supporting Information).

The distances between the two H-bond critical points (*cp*1 and *cp*2) and the N, H, and O nuclei against *RC* are illustrated in the plots of Figure 8. Only the points corresponding to the geometries of the three stationary points have been actually calculated, the smooth curves interconnecting them having a pure graphical function. The plots show the strong symmetrization undergone by the H-bond when going from the two N−H···O and O−H···N ground states toward the TS. Geometrical variations are consistent with a strong confinement of the TS proton electron-density basin along the direction of the bond, the basin becoming symmetrically delimited by the two critical points within the strict range of ±0.30 Å (computed excluding compound **1**). This is a first indication of the equalization of the forces that the N and O atoms exert on the proton in the TS.

The nature of these forces can be more clearly seen from the plots of Figure 9, illustrating how $\rho(cp)$ and $\nabla^2\rho(cp)$ change along *RC*. According to Bader's criteria,[15] both N−H···O and O−H···N ground states are to be classified as rather weak closed-shell interactions of prevalent ionic nature. In fact, and with reference to compounds **2**−**4** which display more symmetrical PT-PES, they are characterized by low $\rho(cp)$ values in the range 0.29−0.42 eÅ^{-3} and by slightly positive $\nabla^2\rho(cp)$ values of 3.1−3.8 eÅ^{-5} (values to be compared with those of the covalent N−H and O−H bonds of $2.1 \le \rho(cp) \le 2.2$ eÅ^{-3} and $-43 \le \nabla^2\rho(cp) \le -41$ eÅ^{-5}). These *cp* values are remarkably different from those measured by X−N methods at 8 K[23d] for the homonuclear O−H···O RAHB of benzoylacetone which, amounting to $\rho(cp) = 0.76$ and 0.89 eÅ^{-3} and $\nabla^2\rho(cp) = -4.5$ and −9.1 eÅ^{-5}, are indicative of a shared three-center-four-electron covalent interaction and, on the contrary, are much more similar to those calculated[24a] for the rather weak electrostatic H-bond of water dimers: $\rho(cp) = 0.133$ eÅ^{-3} and $\nabla^2\rho(cp) = 1.50$ eÅ^{-5}.

These strong differences vanish when considering the TS properties of O−H···O and N−H···O/O−H···N RAHBs: $\langle\rho(cp)\rangle = 1.18[2]$ and $\langle\nabla^2\rho(cp)\rangle = -10[1]$ for ketohydrazones **2**−**5**, and 1.20[4] eÅ^{-3} and −7[1] eÅ^{-5} for the DFT-calculated TS of benzoylacetone.[23e] Therefore, despite the large differences in their ground-state properties, the two TSs appear to be very similar as far as their electron distributions are concerned, being characterized by a same $\rho(cp) \simeq 1.20$ eÅ^{-3}, which is nearly one-half of that of a normal N−H or O−H covalent bond, and by remarkably negative $\nabla^2\rho(cp)$ values. *TSs of both O−H···O and N−H···O/O−H···N RAHBs are then to be classified as shared interactions, that is, as true three-center-four-electron covalent bonds.*

Conclusions

The tautomeric ketohydrazone−azoenol system **II** has turned out to be an almost ideal benchmark for the study of N−H···O/O−H···N LBHBs. The RAHB nature of the system guarantees

(22) (a) Coulson, C. A.; Danielsson, U. *Ark. Fys.* **1954**, *8*, 239. (b) Coulson, C. A.; Danielsson, U. *Ark. Fys.* **1954**, *8*, 245. (c) Pimentel, G. C. *J. Chem. Phys.* **1951**, *19*, 446. (d) Reid, C. *J. Chem. Phys.* **1959**, *30*, 182. (e) Kollman, P. A.; Allen, L. C. *J. Am. Chem. Soc.* **1970**, *92*, 6101. (f) Stevens, E. D.; Lehmann, M. S.; Coppens, P. *J. Am. Chem. Soc.* **1977**, *99*, 2829. (g) Desmeules, P. J.; Allen, L. C. *J. Chem. Phys.* **1980**, *72*, 4731.

(23) (a) Flensburg, C.; Larsen, S.; Stewart, R. F. *J. Phys. Chem.* **1995**, *99*, 10130. (b) Madsen, D.; Flensburg, C.; Larsen, S. *J. Phys. Chem. A* **1998**, *102*, 2177. (c) Mallinson, P. R.; Wozniak, K.; Smith, G. T.; McCormack, K. L. *J. Am. Chem. Soc.* **1997**, *119*, 11502. (d) Madsen, G. K. H.; Iversen, B. B.; Larsen, F. K.; Kapon, M.; Reisner, G. M.; Herbstein, F. H. *J. Am. Chem. Soc.* **1998**, *120*, 10040. (e) Schiøtt, B.; Iversen, B. B.; Madsen, G. H. K.; Bruice, T. C. *J. Am. Chem. Soc.* **1998**, *120*, 12117. (f) Koritsanszky, T. S.; Coppens, P. *Chem. Rev.* **2001**, *101*, 1583.

(24) (a) Page 292 of ref 15. (b) The present classification of strong H-bonds essentially agree with that recently proposed by P. A. Frey (ref 3f).

the formation of H-bonds of relevant strength and provides, in addition to the usual N, H, and O distances, a further precise indicator of such a strength, that is, the π-delocalization index $\langle\lambda\rangle$, while the lack of *N*-substituents in the hydrazone moiety makes it possible to design a set of proper constrain-free substituents (test molecules **1**−**5** of Scheme 1) able to modify the electronic properties of the PT-barrier and to give rise to stable H-bond configurations going from N−H···O to O−H···N through LBHB tautomeric N−H···O/O−H···N bonds.

The property of compounds ***pF*** and ***oF*** of undergoing continuous solid-state N−H···O ⇄ O−H···N exchange, previously predicted on the grounds of qualitative electrostatic-covalent H-bond model[1,4c] considerations, has been fully confirmed by the corresponding variable-temperature X-ray crystallography structural determinations which have determined energy differences between the two H-bond wells of only 0.120(15) and 0.153(23) kcal mol^{-1}, respectively, in favor of the N−H···O configuration. Successive emulation of ***pF*** by DFT quantum-mechanical methods (test molecule **4**) has shown that both energetic and geometric aspects of the molecule and of its intramolecular H-bond can be almost perfectly reproduced.

A generalization of the results obtained for this particular LBHB has been sought by performing DFT calculations along the complete PT-pathway for the set **1**−**5**, followed by a systematic correlative analysis of energies, H-bond and π-conjugated fragment geometries, and H-bond AIM[15] topological properties along the pathway itself. This allowed the establishment of several comprehensive properties of the ketohydrazone−azoenol system in particular, and of the N−H···O/O−H···N RAHB in general, that may shed a new light on the nature of the H-bond in itself:

(a) The focal point of any X−H···Y H-bonded system has to be seen, more than in the variety of bonds it may form, in the structure and properties of its PT-barrier.

(b) Though different chemical substituents can actually produce quite different PT-pathways (Figure 5), all aspects concerning the shape of the PT-barrier can be easily brought together in the frame of the Marcus rate-equilibrium theory,[16b−h] by which any X−H···Y system is fully characterized by the features of its intrinsic PT-barrier, that is, the symmetric barrier occurring when the PAs of X and Y become identical. This barrier represents the lowest possible PT-barrier of the system and determines completely the features of the strongest X−H···Y bond achievable that can therefore be called the *intrinsic H-bond* for that particular X−H···Y system.

(b1) When the intrinsic PT-barrier is lower than the zero-point vibrational level of the proton, the H-bond can be indicated as X···H···Y and variously called single-minimum, single-well, or no-barrier H-bond.[24b] It is a dynamic rather than static structure whose mean (crystallographic) geometry can only be understood in terms of statistical-mechanical averaging over the time.

(b2) When the intrinsic PT-barrier is slightly higher than the zero-point vibrational level, two formally tautomeric H-bonds, X−H···Y and Y−H···X, become possible, jointly called double-minimum, double-well, or low-barrier H-bond.[24b] It can be both a static or dynamic structure, according to how the numeric value of the intrinsic PT-barrier compares with the average kinetic energy of the enviroment. NMR studies in solution normally detect dynamic proton exchange. In crystals, both dynamic exchange and static disorder are possible, which can be discriminated by variable-temperature X-ray crystallography experiments.

(c) With reference to the intrinsic H-bond, the effect of any chemical substitution can only be that of making more and more dissymmetric the PT-barrier (Figure 5). This increasingly splits the two competing H-bonds in

(c1) a higher-energy H-bond which is stronger because closer to the TS structure;

(c2) a lower-energy H-bond (the stable form) which is weaker because farther from the TS structure.

The general effect of barrier dissymmetrization is making weaker and weaker the more stable H-bond till an extreme dissymmetric single-minimum or dissymmetric single-well H-bond is formed (Figure 5-**1**).

(d) For any X−H···Y H-bonded system, the strongest H-bonds can therefore occur only in connection with essentially symmetric PT-barriers where X and Y have the same proton-accepting ability (criterion of PA or pK_a matching[2,3]).

(e) These strong symmetric H-bonds are, of course, those previously identified as chemical leitmotifs in the frame of the electrostatic-covalent H-bond model,[1,4c] that is, [X···H···Y]$^-$ negative-charge-assisted H-bonds [(−)CAHB], [X···H···Y]$^+$ positive-charge-assisted H-bonds [(+)CAHB], [···X···H···Y···] resonance-assisted H-bonds [RAHB], and [AcX−H···YBase ⇄ AcX$^-$···H−Y$^+$Base] positive/negative-charge-assisted H-bonds [(±)CAHB] for both homonuclear (Y = X) and heteronuclear (Y ≠ X) cases.

(f) Present results seem to indicate that a given H-bonded system (such as the N−H···O/O−H···N RAHB) can be more efficiently characterized by the properties of its intrinsic PT-pathway than by a comparative study of all H-bonds it may form when changing its pattern of chemical substituents. A similar simplification could be probably achieved also by monitoring the properties of the TS. These properties appear in fact (with the exclusion of the strongly dissymmetric compound **1**) to be remarkably constant for all other compounds investigated (Figures 6−9). The TS occurs at the same values of π-delocalization ($\langle\lambda\rangle$ = 0.637[5]), reaction coordinate (*RC* = −0.02[4] Å), N···O contact distance (*d*(N···O) = 2.379[4] Å, N−H−O angle (α(N−H−O) = 150[1]°), and AIM critical point parameters ($\rho(cp)$ = 1.18[7] eÅ^{-3}; $\nabla^2\rho(cp)$ = −10[3] eÅ^{-5}), all values which characterize the TS as the strongest three-center-four-electron covalent bond achievable in the present N···H···O RAHB system. These preliminary conclusions seem to open the interesting perspective of a future classification of all H-bonded systems (F−H···F, O−H···O, N−H···O/O−H···N, C−H···O, etc.) on the basis of their intrinsic-barrier and TS properties.

Experimental Section

Variable-Temperature Crystal Structure Analysis. Compounds ***pF*** and ***oF*** were synthesized by one of us (A.L.) by condensation of 4- and 2-fluorobenzenediazonium chloride with β-naphthol in alkaline medium[9a] and recrystallized from ethanol. X-ray diffraction data were collected at four different temperatures (100, 150, 200, and 295 K) on a Nonius KappaCCD diffractometer with graphite-monochromated Mo Kα radiation (λ = 0.71069 Å). Data sets were integrated with the DENZO-SMN package.[25a] Structures were solved by direct methods with the SIR94 package[25b] and refined (SHELXL97[25c]) by full-matrix

least squares with anisotropic non-H and isotropic H atoms. In both structures and at all temperatures, the difference Fourier showed diffuse electron density between the N and O atoms with two maxima from which two proton positions could be identified. Refinement of the two H-atoms with partial occupancy and isotropic thermal parameters fixed at 1.2 times the average of those of the N and O atoms was successfully attempted giving the final occupancy factors displayed for both crystals at all temperatures in Table 2. Difference Fourier maps computed after a further refinement carried out with the exclusion of the tautomeric disordered proton clearly show two maxima at the partial proton positions whose relative intensities are systematically changing with the temperature. Difference Fourier maps for compound ***pF*** are illustrated in Figure 3. Crystal data are given below. Tables of bond distances and angles are given in full as Supporting Information in CIF format and, as a selection, in Table 1. Complete parameters for the N···H···O intramolecular bond are given in Table 2.

Crystal Data for *pF_100*. (1*Z*)-naphthalene-1,2-dione 1-[(4-fluorophenyl)hydrazone], $C_{16}H_{11}FN_2O$, $M_r = 266.27$, monoclinic $P2_1/n$ (no. 14), red, $a = 3.8762(1)$, $b = 27.0486(7)$, $c = 11.6628(3)$ Å, $\beta = 97.646(2)°$, $V = 1211.92(5)$ Å^3, $Z = 4$, $D_{calc} = 1.46$ g cm^{-3}, $\mu = 1.04$ cm^{-1}, and $T = 100$ K. 2677 unique measured reflections were used in the refinement, out of which 2188 with $I \geq 2\sigma(I)$ were considered observed. R (on F^2, observed reflections) = 0.040, R_w (all reflections) = 0.110, and $S = 1.05$.

Crystal Data for *pF_150*. (1*Z*)-naphthalene-1,2-dione 1-[(4-fluorophenyl)hydrazone], $C_{16}H_{11}FN_2O$, $M_r = 266.27$, monoclinic $P2_1/n$ (no. 14), red, $a = 3.8978(1)$, $b = 27.0734(8)$, $c = 11.6656(3)$ Å, $\beta = 97.558(2)°$, $V = 1220.34(5)$ Å^3, Z = 4, $D_{calc} = 1.45$ g cm^{-3}, $\mu = 1.03$ cm^{-1}, and $T = 150$ K. 2567 unique measured reflections were used in the refinement, out of which 2099 with $I \geq 2\sigma(I)$ were considered observed. R (on F^2, observed reflections) = 0.043, R_w (all reflections) = 0.114, and $S = 1.07$.

Crystal Data for *pF_200*. (1*Z*)-naphthalene-1,2-dione 1-[(4-fluorophenyl)hydrazone], $C_{16}H_{11}FN_2O$, $M_r = 266.27$, monoclinic $P2_1/n$ (no. 14), red, $a = 3.9237(1)$, $b = 27.1083(8)$, $c = 11.6690(2)$ Å, $\beta = 97.520(2)°$, $V = 1230.50(5)$ Å^3, $Z = 4$, $D_{calc} = 1.44$ g cm^{-3}, $\mu = 1.02$ cm^{-1}, and $T = 200$ K. 2712 unique measured reflections were used in the refinement, out of which 2104 with $\geq 2\sigma(I)$ were considered observed. R (on F^2, observed reflections) = 0.042, R_w (all reflections) = 0.114, and $S = 1.04$.

Crystal Data for *pF_295*. (1*Z*)-naphthalene-1,2-dione 1-[(4-fluorophenyl)hydrazone], $C_{16}H_{11}FN_2O$, $M_r = 266.27$, monoclinic $P2_1/n$ (no. 14), red, $a = 3.9825(1)$, $b = 27.1459(10)$, $c = 11.6686(4)$ Å, $\beta = 97.598(2)°$, $V = 1250.40(7)$ Å^3, $Z = 4$, $D_{calc} = 1.41$ g cm^{-3}, $\mu = 1.00$ cm^{-1}, and $T = 295$ K. 2560 unique measured reflections were used in the refinement, out of which 1923 with $I \geq 2\sigma(I)$ were considered observed. R (on F^2, observed reflections) = 0.048, R_w (all reflections) = 0.125, and $S = 1.12$.

Crystal Data for *oF_100*. (1*Z*)-naphthalene-1,2-dione 1-[(2-fluorophenyl)hydrazone], $C_{16}H_{11}FN_2O$, $M_r = 266.27$, orthorhombic $Pca2_1$ (no. 29), red, $a = 23.6288(6)$, $b = 7.2487(2)$, $c = 7.1894(2)$ Å, $V = 1231.39(6)$ Å^3, Z = 4, $D_{calc} = 1.44$ g cm^{-3}, $\mu = 1.02$ cm^{-1}, and $T = 100$ K. 2645 unique measured reflections were used in the refinement, out of which 2359 with $I \geq 2\sigma(I)$ were considered observed. R (on F^2, observed reflections) = 0.036, R_w (all reflections) = 0.080, and $S = 1.07$.

Crystal Data for *oF_150*. (1*Z*)-naphthalene-1,2-dione 1-[(2-fluorophenyl)hydrazone], $C_{16}H_{11}FN_2O$, $M_r = 266.27$, orthorhombic $Pca2_1$ (no. 29), red, $a = 23.6614(7)$, $b = 7.2580(2)$, $c = 7.2182(2)$ Å, $V = 1239.61(6)$ Å^3, Z = 4, $D_{calc} = 1.43$ g cm^{-3}, $\mu = 1.01$ cm^{-1}, and $T = 150$ K. 2693 unique measured reflections were used in the refinement, out of which 2217 with $I \geq 2\sigma(I)$ were considered observed. R (on F^2, observed reflections) = 0.039, R_w (all reflections) = 0.086, and $S = 1.06$.

Crystal Data for *oF_200*. (1*Z*)-naphthalene-1,2-dione 1-[(2-fluorophenyl)hydrazone], $C_{16}H_{11}FN_2O$, $M_r = 266.27$, orthorhombic $Pca2_1$ (no. 29), red, $a = 23.7049(9)$, $b = 7.2711(3)$, $c = 7.2535(3)$ Å, $V = 1250.22(9)$ Å^3, $Z = 4$, $D_{calc} = 1.42$ g cm^{-3}, $\mu = 1.00$ cm^{-1}, and $T = 200$ K. 2317 unique measured reflections were used in the refinement, out of which 2096 with $I \geq 2\sigma(I)$ were considered observed. R (on F^2, observed reflections) = 0.039, R_w (all reflections) = 0.091, and $S = 1.13$.

Crystal Data for *oF_295*. (1*Z*)-naphthalene-1,2-dione 1-[(2-fluorophenyl)hydrazone], $C_{16}H_{11}FN_2O$, $M_r = 266.27$, orthorhombic $Pca2_1$ (no. 29), red, $a = 23.7800(10)$, $b = 7.2962(4)$, $c = 7.3283(5)$ Å, $V = 1271.49(12)$ Å^3, $Z = 4$, $D_{calc} = 1.39$ g cm^{-3}, $\mu = 0.99$ cm^{-1}, and $T = 295$ K. 2645 unique measured reflections were used in the refinement, out of which 2359 with $I \geq 2\sigma(I)$ were considered observed. R (on F^2, observed reflections) = 0.048, R_w (all reflections) = 0.107, and $S = 1.23$.

Computational Details. The problem of choosing an appropriate level of theory for strong H-bonds, particularly of RAHB type, has been investigated with some systematism by several authors.[26] It is generally recognized that the H-bond geometry of RAHB molecules cannot be reproduced at the Hartree−Fock level[26a] and that electron correlation can be satisfactorily accounted for both by ab initio MP2 (or higher) methods[27a,b] and by density functional theory (DFT) methods[11] with hybrid functional, in particular B3LYP.[27c,d] As for the basis set, a systematic investigation carried out by McAllister[28] has suggested that 6-31+G(d,p) is most probably the best compromise between computational accuracy and costs for the general study of LBHBs. In view of these considerations and of the fact that DFT methods are faster, all calculations were accomplished by using the Gaussian 98[29a] suite of programs at the B3LYP/6-31+G(d,p)// B3LYP/6-31+G(d,p) level of theory.

Geometry optimization for all test molecules **1**−**5** was accomplished assuming molecular planarity (point group C_S), an assumption confirmed a posteriori by frequency calculations on the optimized geometries. TSs of the PT reaction were located by the QST2 method.[14] PT-pathways of 23 points each were obtained by QST3[14] for molecules **2**−**5**. For molecule **1**, having a strongly dissymmetric barrier, the QST2[14] method with the "path" option was used because it was found to give a more even distribution of points on the two sides of the TS

(25) (a) Otwinowski, Z.; Minor, W. In *Methods Enzymol.*; Carter, C. W., Jr., Sweets, R. M., Eds.; Macromolecular Crystallography, Vol. 276, Part A; Academic Press: San Diego, CA, 1997; p 307. (b) Altomare, A.; Cascarano, G.; Giacovazzo, C.; Guagliardi, A.; Burla, M. C.; Polidori, G.; Camalli, M. *J. Appl. Crystallogr.* **1994**, *27*, 435. (c) Sheldrick, G. M. *SHELXL97, Program for crystal structure refinement*; University of Göttingen: Göttingen, Germany, 1997.

(26) (a) Frisch, M. J.; Scheiner, A. C.; Schaefer, H. F., III; Binkley, J. S. *J. Chem. Phys.* **1985**, *82*, 4194. (b) Dannenberg, J. J.; Rios, R. *J. Phys. Chem.* **1994**, *98*, 6714. (c) Barone, V.; Adamo, C. *J. Chem. Phys.* **1996**, *105*, 11007. (d) Buemi, G.; Zuccarello, F. *J. Chem. Soc., Faraday Trans.* **1996**, *92*, 347. (e) Buemi, G.; Zuccarello, F. *Electron. J. Theor. Chem.* **1997**, *2*, 302. (f) Chung, G.; Kwon, O.; Kwon, Y. *J. Phys Chem. A* **1997**, *101*, 4628. (g) Kobko, N.; Paraskevas, L.; del Rio, E.; Dannenberg, J. J. *J. Am. Chem. Soc.* **2001**, *123*, 4348.

(27) (a) Here, W. J.; Radom, L.; Schleyer, P. v. R.; Pople, J. A. *Ab Initio Molecular Orbital Theory*; Wiley-Interscience: New York, 1986; see also references therein. (b) Møller, C.; Plesset, M. S. *Phys. Rev.* **1934**, *46*, 618. (c) Becke, A. D. *J. Chem. Phys.* **1993**, *98*, 5648. (d) Lee, C.; Yang, Y.; Parr, R. G. *Phys. Rev. B* **1988**, *37*, 785.

(28) (a) Pan, Y.; McAllister, M. A. *J. Mol. Struct. (THEOCHEM)* **1998**, *427*, 221. (b) McAllister, M. A. *J. Mol. Struct. (THEOCHEM)* **1998**, *427*, 39. (c) Smallwood, C. J.; McAllister, M. A. *Can. J. Chem.* **1997**, *75*, 1195.

(29) (a) Frisch, M. J.; Trucks, G. W.; Schlegel, H. B.; Scuseria, G. E.; Robb, M. A.; Cheeseman, J. R.; Zakrzewski, V. G.; Montgomery, J. A., Jr.; Stratmann, R. E.; Burant, J. C.; Dapprich, S.; Millam, J. M.; Daniels, A. D.; Kudin, K. N.; Strain, M. C.; Farkas, O.; Tomasi, J.; Barone, V.; Cossi, M.; Cammi, R.; Mennucci, B.; Pomelli, C.; Adamo, C.; Clifford, S.; Ochterski, J.; Petersson, G. A.; Ayala, P. Y.; Cui, Q.; Morokuma, K.; Malick, D. K.; Rabuck, A. D.; Raghavachari, K.; Foresman, J. B.;. Cioslowski, J.; Ortiz, J. V.; Baboul, A. G.; Stefanov, B. B.; Liu, G.; Liashenko, A.; Piskorz, P.; Komaromi, I.; Gomperts, R.; Martin, R. L.; Fox, D. J.; Keith, T.; Al-Laham, M. A.; Peng, C. Y.; Nanayakkara, A.; Gonzalez, C.; Challacombe, M.; Gill, P. M. W.; Johnson, B.; Chen, W.; Wong, M. W.; Andres, J. L.; Gonzalez, C.; Head-Gordon, M.; Replogle, E. S.; Pople, J. A. *GAUSSIAN 98*, Revision A.7; Gaussian, Inc.: Pittsburgh, PA, 1998. (b) Stefanov, B. B.; Cioslowski, J, *Mol. Phys.* **1995**, *84*, 707.

(all calculations at the previously indicated level of theory). Final AIM[15] calculations were performed using the routines written by Cioslowski and co-workers[29b] as implemented in Gaussian 98.[29a] Final geometries and energies for all optimized stationary points are given in Tables S3 and S4 of Supporting Information.

Acknowledgment. This paper is dedicated to the memory of Prof. Jan Kroon (University of Utrecht, The Netherlands), who prematurely died in May 2001, in acknowledgment of his great contribution to hydrogen bond studies in chemistry and biology by diffraction, ab initio, and molecular dynamics methods. We thank CINECA, Casalecchio di Reno (Bologna), for free use of its IBM SP3 computer facility and much assistance in the use of programs and INSTM (Florence) for financial support of our computational activities.

Supporting Information Available: Table of AIM topological parameters; comparison of the experimental and DFT-calculated geometries for compound ***pF***; final geometries and energies for all the DFT-optimized stationary points; ORTEP plots for ***pF*** and ***oF*** at 150, 200, and 295 K; comparison of the PT activation energies calculated by DFT and Marcus methods (PDF); X-ray crystallographic files (CIF). This material is available free of charge via the Internet at http://pubs.acs.org.

JA020589X